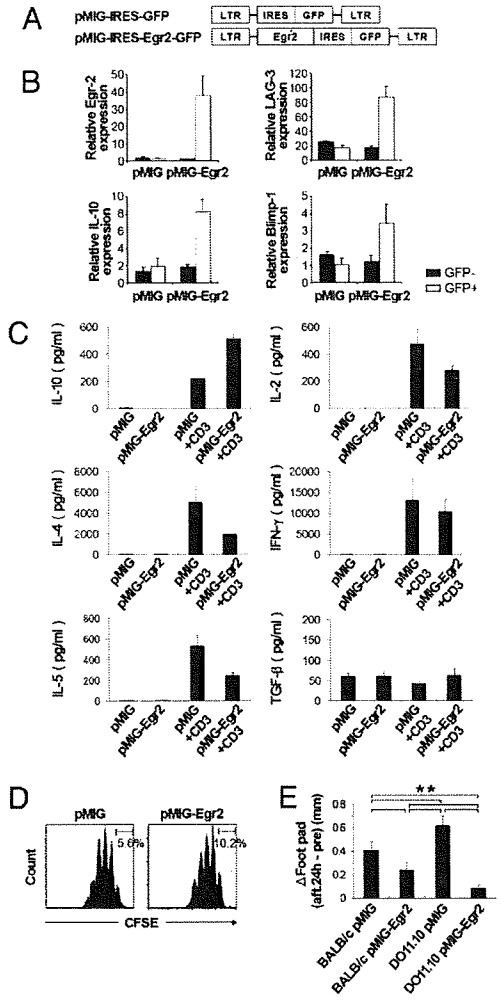

Fig. 3. Retroviral transduction of Egr-2 into naïve T cells. (*A*) Retroviral constructs for the transduction of Egr-2. (*B*) Ectopic Egr-2 expression induced the expression of LAG-3, IL-10, and Blimp-1. Quantitative PCR analyses of gene expression in sorted retrovirally transduced cell populations stimulated for 5 days with soluble anti-CD3 mAb (1 μg/mL). The results are the means of three independent experiments. (*C*) Cytokines in the culture supernatants of pMIG- and pMIG-Egr2-transduced $CD4^+GFP^+$ T cells stimulated for 48 h with or without plate-coated anti-CD3 mAb. The results are the means of three independent experiments. (*D*) Suppression of naïve carboxyfluorescein diacetate succinimidyl ester (CFSE)-labeled $CD4^+CD25^-CD45RB^{high}$ T cells by Egr-2-transduced T cells in vitro. Naïve $CD4^+CD25^-CD45RB^{high}$ $Thy1.1^+$ T cells were labeled with CFSE and cultured with the indicated retrovirally transduced $Thy1.2^+$ T cells and irradiated whole splenocytes plus anti-CD3 mAb. Representative data from three independent experiments are shown. (*E*) Antigen-specific suppression of the delayed-type hypersensitivity (DTH) response by Egr2-transduced $CD4^+$ T cells. Six days after primary immunization, FACS-sorted pMIG- or pMIG-Egr2-transduced $CD4^+$ T cells (1×10^6) from BALB/c or DO11.10 mice were transferred adoptively via i.v. injection into BALB/c mice. Two days after adoptive cell transfer, DTH response in the footpad was induced. Footpad thickness was determined 24 h later; $n = 6$ per group. All error bars represent ±SD. **, $P < 0.01$.

$CD4^+CD45RB^{low}$ subset in an IL-10-dependent manner (36). The suppressive activity was independent of $CD4^+CD25^+$ Tregs, because $CD4^+CD25^+$ T-cell-depleted $CD4^+CD25^-CD45RB^{low}$ T cells retained suppressive activity (37). The present findings that $CD4^+CD25^-CD45RB^{low}LAG3^+$ T cells exhibited stronger suppressive activity than $CD4^+CD25^-CD45RB^{low}LAG3^-$ T cells indicated that the suppressive activity of $CD4^+CD25^-CD45RB^{low}$ T cells was confined mainly to $CD4^+CD25^-CD45RB^{low}LAG3^+$ T cells expressing high levels of Egr-2. The association between LAG-3 and IL-10 production was consistent with previous observations (25). In addition to $CD4^+CD25^-CD45RB^{low}$ T cells, a decade of active research has focused on IL-10-producing type 1 regulatory T cells (Tr1) induced in vitro by antigenic stimulation (14). $CD4^+CD25^-LAG3^+$ Tregs were probably different from Tr1 in that $CD4^+CD25^-LAG3^-$ Tregs did not produce TGF-β and IL-5 (14). However, the precise relationships between $CD4^+CD25^-LAG3^+$ Tregs and Tr1 should be investigated further, because an optimal stimulation may induce TGF-β and IL-5 production in $CD4^+CD25^-LAG3^+$ Tregs.

In this study, the suppressive phenotype of $CD4^+CD25^-LAG3^+$ Tregs was determined by Egr-2. Egr-2 transduced T cells exhibited antigen-specific immunosuppressive capacity in vivo. Forced expression of Egr-2 in $CD4^+$ T cells induced the expression of LAG3, IL-10, and Blimp-1 genes. These results are consistent with the recent findings that T-cell-specific Blimp-1 conditional knockout mice showed impaired IL-10 production and increased IL-2 production in activated $CD4^+$ T cells and that they developed spontaneous colitis (38, 39).

The extrathymic development of IL-10-secreting T cells already has been reported (40). The severe decrease of $CD4^+CD25^-LAG3^+$ Tregs in GF mice shows the importance of environmental microbiota for the development of $CD4^+CD25^-LAG3^+$ Tregs. Germfree models represent an important tool for uncovering the function of gut microbiota, especially their effects on mucosal immunity (33, 34). Recently, gut-associated lymphoid tissue has been demonstrated to be a preferential site for the peripheral induction of $Foxp3^+$ regulatory T cells (41). In particular, dendritic cells (DCs) expressing $CD103^+$ from the lamina propria of the small intestine and from the mesenteric lymph node can induce $Foxp3^+$ T cells (42). Plasmacytoid DCs presenting dietary antigens are responsible for induction of oral tolerance and immune suppression affecting both $CD4^+$ and $CD8^+$ responses (43). The precise mechanisms of the development of $CD4^+CD25^-LAG3^+$ Tregs by environmental microbiota and antigen-presenting cells should be examined further.

Recent genome-wide association studies reported SNPs on chromosome 10q21 with a strong association to Crohn's disease (44, 45), a common form of chronic inflammatory bowel disease (IBD). The associated intergenic region is flanked by Egr-2, suggesting that this genetic variation could regulate Egr-2 expression. The characteristically high production level of IL-10 by Egr-2-dependent $CD4^+CD25^-$ T cells suggests that this Treg population may contribute to the control of organ inflammation. Moreover, T-cell-specific Egr-2-deficient mice showed autoimmune disease characterized by the enhanced expression of proinflammatory cytokines and massive infiltration of T cells into multiple organs (46). By exploiting the capacity of Egr-2-dependent $CD4^+CD25^-LAG3^+$ Tregs to produce a large amount of IL-10, they can be useful for antigen-specific treatment of inflammatory disease, in particular IBD.

Materials and Methods

Mice. BALB/c and C57BL/6 mice were purchased from Japan SLC. C57BL/6 recombinase-activating gene 1 (*rag-1*) deficient ($RAG1^{-/-}$) mice and TCR transgenic OT-II mice were purchased from Taconic. $RAG1^{-/-}$ mice were housed in microisolator cages with sterile filtered air. TCR transgenic DO11.10 mice, IL-10-deficient ($IL\text{-}10^{-/-}$) mice (47), B6.Thy1.1 mice, and Foxp3-eGFP mice (48) were purchased from Jackson Laboratory. RIP-mOVA (49) mice and B6.$Foxp3^{sfl/+}$ female mice were purchased from Jackson Laboratory and backcrossed with C57BL/6 males. B6.$Foxp3^{sfl/Y}$ male mice (11) were used at 21 days of age. All mice except B6.$Foxp3^{sfl/Y}$ and B6.$Foxp3^{sfl/+}$ were used at >7 weeks of age. All animal experiments were conducted in accordance with institutional and national guidelines.

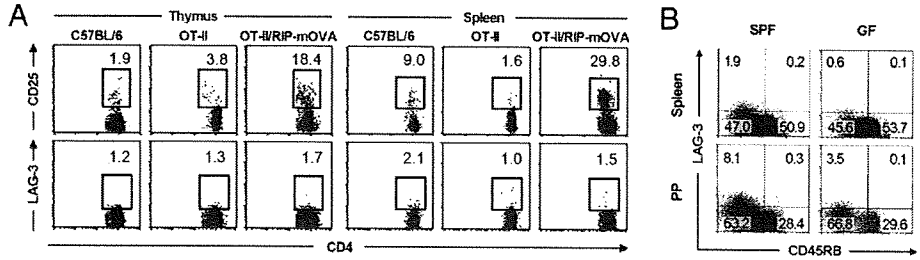

Fig. 4. Development of CD4$^+$CD25$^-$LAG3$^-$ T cells. (*A*) Flow cytometry of LAG-3 and CD25 expression in the thymus and spleen of OT-II TCR transgenic mice with or without the RIP-mOVA transgene. *Upper* and *Lower* plots are gated on CD4$^+$Vβ5.1/5.2$^+$ and CD4$^+$CD25$^-$Vβ5.1/5.2$^+$ T cells, respectively. Representative FACS dot plots from three independent experiments are shown. (*B*) Flow cytometry of LAG-3 and CD45RB expression in the spleen and Peyer's patch (PP) of specific-pathogen-free (SPF) (*Left*) and germfree (GF) (*Right*) mice gated on CD4$^+$CD25$^-$ T cells. Representative FACS dot plots from at least three independent experiments are shown.

Reagents. Purified and conjugated antibodies were purchased from BD Pharmingen, eBioscience, or Miltenyi Biotec, and recombinant cytokines were obtained from R&D Systems. See *SI Materials and Methods* for details.

RNA Isolation, cDNA Synthesis, and Quantitative Real-Time PCR. Total T cell RNA was prepared using an RNeasy Micro Kit (Qiagen). RNA was reverse-transcribed to cDNA, and quantitative real-time PCR analysis was performed as described in *SI Materials and Methods*. Relative RNA abundance was determined based on control β-actin abundance.

DNA Microarray Analysis. Total RNA of CD4$^+$CD25$^+$, CD4$^+$CD25$^-$CD45RB^{low}LAG3$^+$, CD4$^+$CD25$^-$CD45RB^{low}LAG3$^-$, and CD4$^+$CD25$^-$CD45RB^{high} FACS-purified T cells from C57BL/6 mice were harvested as described above and then prepared for Affymetrix microarray analysis as described in *SI Materials and Methods*. The data were analyzed using Bioconductor (version 1.9) (50) statistical software R and GeneSpring GX version 7.3.1 (Silicon Genetics). All microarray data have been deposited in the ArrayExpress database (http://www.ebi.ac.uk/arrayexpress) under accession number E-MEXP-1343.

Proliferation Assay. Each T cell population (1×10^5 cells per well) purified from C57BL/6 mice was cultured in U-bottomed 96-well plates coated anti-CD3 mAb for 72 h. ^{3}H-thymidine (1 μCi per well; NEN Life Science Products) was added during the last 15 h of culture. Cells were harvested and counted using a β^- counter. Results were expressed as the mean $\pm$ SD of triplicate cultures.

Suppression Assay. FACS-purified CD4$^+$CD25$^-$CD45RB^{high} T cells isolated from B6.Thy1.1 mice were stained with 5 μM carboxyfluorescein diacetate succinimidyl ester (CFSE) by incubating them for 10 min at 37 °C. The reaction was quenched by washing in ice-cold RPMI medium 1640 supplemented with 10% FCS. The CFSE-labeled CD4$^+$CD25$^-$CD45RB^{high} T cells (5×10^4) were cocultured with 1×10^5 irradiated whole splenocytes in the presence or absence of 5×10^4 retrovirally gene-transduced CD4$^+$GFP$^+$-sorted T cells or CD4$^+$CD25$^-$CD45RB^{low}LAG3$^{+\ or-}$ T cells from C57BL/6 mice in U-bottomed 96-well plates in the presence of 1.0 μg/mL anti-CD3 mAb. After 72 h, cells were analyzed by flow cytometry and gated on Thy1.1$^+$CD4$^+$ cells.

Colitis Model. Syngenic purified CD4$^+$CD25$^-$CD45RB^{high} T cells (1×10^5), described above, from C57BL/6 mice were injected i.p. into RAG1$^{-/-}$ mice alone or in combination with 1×10^5 wild-type CD4$^+$CD25$^-$CD45RB^{low}LAG3$^{+\ or-}$ or IL-10$^{-/-}$ CD4$^+$CD25$^-$CD45RB^{low}LAG3$^+$ T cells. Control mice received PBS. Mice were observed daily and weighed weekly. Seven weeks after cell transfer, the mice were killed, and sections of the colons were stained with hematoxylin and eosin. Mice were killed to assess the severity of colitis as described in *SI Materials and Methods*.

Cytokine Detection. Supernatants from cultures of CD4$^+$ T cells untreated or stimulated by plate-bound anti-CD3 (5 μg/mL) for 48 h or 5 days were harvested and pooled, and IL-2, IL-4, IL-5, IL-10, IFN-γ, and TGF-β concentrations were measured using a commercially available LINCOplex Mouse Cytokine kit (Linco Research) using fluorescently labeled microsphere beads and a Luminex reader according to the manufacturer's instructions at GeneticLabo. Raw data (mean fluorescence intensities) from the beads were analyzed using MasterPlex QT version 2.5 software (Hitachi) to obtain concentration values. All samples were run in duplicate, and results were obtained three times.

DTH Assay. BALB/c mice were immunized with OVA 6 days before the transfer of gene-transduced T cells. Retroviral gene transduction to CD4$^+$ T cells has been reported (51). The experimental groups consisted of CD4$^+$ T cells from BALB/c or DO11.10 mice transduced with pMIG or pMIG-Egr2. In accordance with our previous experiments (30, 31), the average transduction efficiency was $\approx$50%. The GFP-positive fraction of the transduced CD4$^-$ T cells were sorted with FACSAria and transferred to immunized mice. OVA was rechallenged to the footpad 2 days after the transfer, and footpad swelling was measured 24 h later. Detailed protocols are described in *SI Materials and Methods*.

Statistical Analysis. Statistical significance was analyzed using Statview software (SAS Institute). Body weight changes were analyzed by repeated measures two-way ANOVA followed by Bonferroni post test. Colitis scores, quantitative histology, and DTH responses were analyzed with the Mann–Whitney, Scheffé, and Bonferroni tests, respectively. Differences were considered statistically significant with *, $P < 0.05$ and **, $P < 0.01$.

ACKNOWLEDGMENTS. We thank K. Watada for excellent technical assistance. Flow cytometry analysis and cell sorting were done in the Department of Transfusion Medicine and Immunohematology, University of Tokyo, Japan. This work was supported by grants from the Japan Society for the Promotion of Science, Ministry of Health, Labor and Welfare, and the Ministry of Education, Culture, Sports, Science and Technology (MEXT) (in part by Global COE Program Chemical Biology of the Diseases, by the MEXT), Japan.

1. Starr TK, Jameson SC, Hogquist KA (2003) Positive and negative selection of T cells. *Annu Rev Immunol* 21:139–176.
2. Hogquist KA, Baldwin TA, Jameson SC (2005) Central tolerance: Learning self-control in the thymus. *Nat Rev Immunol* 5:772–782.
3. Chen Z, Benoist C, Mathis D (2005) How defects in central tolerance impinge on a deficiency in regulatory T cells. *Proc Natl Acad Sci USA* 102:14735–14740.
4. Roncarolo MG, et al. (2006) Interleukin-10-secreting type 1 regulatory T cells in rodents and humans. *Immunol Rev* 212:28–50.
5. Fife BT, Bluestone JA (2008) Control of peripheral T-cell tolerance and autoimmunity via the CTLA-4 and PD-1 pathways. *Immunol Rev* 224:166–182.
6. Kalinski P, Moser M (2005) Consensual immunity: Success-driven development of T-helper-1 and T-helper-2 responses. *Nat Rev Immunol* 5:251–260.
7. Kano S, et al. (2008) The contribution of transcription factor IRF1 to the interferon-γ–interleukin 12 signaling axis and T_H1 versus T_H-17 differentiation of CD4$^+$ T cells. *Nat Immunol* 9:34–41.
8. Dong C (2008) TH17 cells in development: An updated view of their molecular identity and genetic programming. *Nat Rev Immunol* 8:337–348.
9. Hori S, Nomura T, Sakaguchi S (2003) Control of regulatory T cell development by the transcription factor Foxp3. *Science* 299:1057–1061.
10. Sakaguchi S, Powrie F (2007) Emerging challenges in regulatory T cell function and biology. *Science* 317:627–629.
11. Brunkow ME, et al. (2001) Disruption of a new forkhead/winged-helix protein, scurfin, results in the fatal lymphoproliferative disorder of the scurfy mouse. *Nat Genet* 27:68–73.
12. Liston A, Lesage S, Wilson J, Peltonen L, Goodnow CC (2003) Aire regulates negative selection of organ-specific T cells. *Nat Immunol* 4:350–354.
13. Anderson MS, et al. (2005) The cellular mechanism of Aire control of T cell tolerance. *Immunity* 23:227–239.
14. Groux H, et al. (1997) A CD4$^+$ T-cell subset inhibits antigen-specific T-cell responses and prevents colitis. *Nature* 389:737–742.

15. Barrat FJ, et al. (2002) In vitro generation of interleukin 10-producing regulatory CD4+ T cells is induced by immunosuppressive drugs and inhibited by T helper type 1 (Th1)- and Th2-inducing cytokines. *J Exp Med* 195:603–616.
16. Battaglia M, Gregori S, Bacchetta R, Roncarolo MG (2006) Tr1 cells: From discovery to their clinical application. *Semin Immunol* 18:120–127.
17. Roncarolo MG, Battaglia M (2007) Regulatory T-cell immunotherapy for tolerance to self antigens and alloantigens in humans. *Nat Rev Immunol* 7:585–598.
18. Schwartz RH (2003) T cell anergy. *Annu Rev Immunol* 21:305–334.
19. Mueller DL (2004) E3 ubiquitin ligases as T cell anergy factors. *Nat Immunol* 5:883–890.
20. Heissmeyer V, et al. (2004) Calcineurin imposes T cell unresponsiveness through targeted proteolysis of signaling proteins. *Nat Immunol* 5:255–265.
21. Safford M, et al. (2005) Egr-2 and Egr-3 are negative regulators of T cell activation. *Nat Immunol* 6:472–480.
22. Topilko P, et al. (1994) Krox-20 controls myelination in the peripheral nervous system. *Nature* 371:796–799.
23. Workman CJ, Vignali DA (2003) The CD4-related molecule, LAG-3 (CD223), regulates the expansion of activated T cells. *Eur J Immunol* 33:970–979.
24. Workman CJ, et al. (2004) Lymphocyte activation gene-3 (CD223) regulates the size of the expanding T cell population following antigen activation in vivo. *J Immunol* 172:5450–5455.
25. Huang CT, et al. (2004) Role of LAG-3 in regulatory T cells. *Immunity* 21:503–513.
26. Workman CJ, Rice DS, Dugger KJ, Kurschner C, Vignali DA (2002) Phenotypic analysis of the murine CD4-related glycoprotein, CD223 (LAG-3). *Eur J Immunol* 32:2255–2263.
27. Lehmann J, et al. (2002) Expression of the integrin $\alpha_E\beta_7$ identifies unique subsets of $CD25^+$ as well as $CD25^-$ regulatory T cells. *Proc Natl Acad Sci USA* 99:13031–13036.
28. Ochi H, et al. (2006) Oral CD3-specific antibody suppresses autoimmune encephalomyelitis by inducing $CD4^+CD25^-LAP^+$ T cells. *Nat Med* 12:627–635.
29. Harris JE, et al. (2004) Early growth response gene-2, a zinc-finger transcription factor, is required for full induction of clonal anergy in $CD4^+$ T cells. *J Immunol* 173:7331–7338.
30. Fujio K, et al. (2004) Nucleosome-specific regulatory T cells engineered by triple gene transfer suppress a systemic autoimmune disease. *J Immunol* 173:2118–2125.
31. Fujio K, et al. (2006) Gene therapy of arthritis with TCR isolated from the inflamed paw. *J Immunol* 177:8140–8147.
32. Coutinho A, Caramalho I, Seixas E, Demengeot J (2005) Thymic commitment of regulatory T cells is a pathway of TCR-dependent selection that isolates repertoires undergoing positive or negative selection. *Curr Top Microbiol Immunol* 293:43–71.
33. Tlaskalova-Hogenova H, et al. (2004) Commensal bacteria (normal microflora), mucosal immunity and chronic inflammatory and autoimmune diseases. *Immunol Lett* 93:97–108.
34. Wen L, et al. (2008) Innate immunity and intestinal microbiota in the development of type 1 diabetes. *Nature* 455:1109–1113.
35. Aranda R, et al. (1997) Analysis of intestinal lymphocytes in mouse colitis mediated by transfer of $CD4^+$, $CD45RB^{high}$ T cells to SCID recipients. *J Immunol* 158:3464–3473.
36. Asseman C, Mauze S, Leach MW, Coffman RL, Powrie F (1999) An essential role for interleukin 10 in the function of regulatory T cells that inhibit intestinal inflammation. *J Exp Med* 190:995–1004.
37. Annacker O, et al. (2001) $CD25^-$ $CD4^+$ T cells regulate the expansion of peripheral CD4 T cells through the production of IL-10. *J Immunol* 166:3008–3018.
38. Kallies A, et al. (2006) Transcriptional repressor Blimp-1 is essential for T cell homeostasis and self-tolerance. *Nat Immunol* 7:466–474.
39. Martins GA, et al. (2006) Transcriptional repressor Blimp-1 regulates T cell homeostasis and function. *Nat Immunol* 7:457–465.
40. Maynard CL, et al. (2007) Regulatory T cells expressing interleukin 10 develop from $Foxp3^+$ and $Foxp3^-$ precursor cells in the absence of interleukin 10. *Nat Immunol* 8:931–941.
41. Belkaid Y, Oldenhove G (2008) Tuning microenvironments: Induction of regulatory T cells by dendritic cells. *Immunity* 29:362–371.
42. Coombes JL, et al. (2007) A functionally specialized population of mucosal $CD103^+$ DCs induces Foxp3+ regulatory T cells via a TGF-β- and retinoic acid-dependent mechanism. *J Exp Med* 204:1757–1764.
43. Goubier A, et al. (2008) Plasmacytoid dendritic cells mediate oral tolerance. *Immunity* 29:464–475.
44. Rioux JD, et al. (2007) Genome-wide association study identifies new susceptibility loci for Crohn disease and implicates autophagy in disease pathogenesis. *Nat Genet* 39:596–604.
45. Wellcome Trust Case Control Consortium (2007) Genome-wide association study of 14,000 cases of seven common diseases and 3,000 shared controls. *Nature* 447:661–678.
46. Zhu B, et al. (2008) Early growth response gene 2 (Egr-2) controls the self-tolerance of T cells and prevents the development of lupuslike autoimmune disease. *J Exp Med* 205:2295–2307.
47. Berg DJ, et al. (1996) Enterocolitis and colon cancer in interleukin-10-deficient mice are associated with aberrant cytokine production and CD4 TH1-like responses. *J Clin Invest* 98:1010–1020.
48. Haribhai D, et al. (2007) Regulatory T cells dynamically control the primary immune response to foreign antigen. *J Immunol* 178:2961–2972.
49. Kurts C, et al. (1996) Constitutive class I-restricted exogenous presentation of self antigens in vivo. *J Exp Med* 184:923–930.
50. Gentleman RC, et al. (2004) Bioconductor: Open software development for computational biology and bioinformatics. *Genome Biol* 5:R80.
51. Fujio K, et al. (2000) Functional reconstitution of class II MHC-restricted T cell immunity mediated by retroviral transfer of the $\alpha\beta$ TCR complex. *J Immunol* 165:528–532.

Nicked β2-glycoprotein I binds angiostatin 4.5 (plasminogen kringle 1-5) and attenuates its antiangiogenic property

Hisako Nakagawa,[1] Shinsuke Yasuda,[1] Eiji Matsuura,[2] Kazuko Kobayashi,[2] Masahiro Ieko,[3] Hiroshi Kataoka,[1] Tetsuya Horita,[1] Tatsuya Atsumi,[1] and Takao Koike[1]

[1]Department of Medicine II, Hokkaido University Graduate School of Medicine, Sapporo; [2]Department of Cell Chemistry, Okayama University Graduate School of Medicine, Dentistry, and Pharmaceutical Sciences, Okayama; and [3]Department of Internal Medicine, School of Dentistry, Health Sciences University of Hokkaido, Ishikari-Tobetsu, Hokkaido, Japan

Angiostatin was first discovered as a plasminogen fragment with antitumor/antiangiogenic property. One of the angiostatin isoforms, that is, angiostatin 4.5 (AS4.5), consisting of plasminogen kringle 1 to 4 and a most part of kringle 5, is produced by autoproteolysis and present in human plasma. β2-glycoprotein I (β2GPI) is proteolytically cleaved by plasmin in its domain V (nicked β2GPI), resulting in binding to plasminogen. Antiangiogenic properties have been recently reported in nicked β2GPI as well as in intact β2GPI at higher concentrations. In the present study, we found significant binding of nicked β2GPI to AS4.5 ($K_D = 3.27 \times 10^6\ M^{-1}$). Via this binding, nicked β2GPI attenuates the antiangiogenic functions of AS4.5 in the proliferation of arterial/venous endothelial cells, in the extracellular matrix invasion and the tube formation of venous endothelial cells, and in vivo angiogenesis. In contrast, intact β2GPI does not bind to AS4.5 or inhibit its antiangiogenic activity. Thus, nicked β2GPI exerts dual effects on angiogenesis, that is, nicked β2GPI promotes angiogenesis in the presence of AS4.5, whereas nicked β2GPI inhibits angiogenesis at concentrations high enough to neutralize AS4.5. Our data suggest that plasmin-nicked β2GPI promotes angiogenesis by interacting with plasmin-generated AS4.5 in sites of increased fibrinolysis such as thrombus. (Blood. 2009;114:2553-2559)

Introduction

Angiogenesis is the formation of a new capillary network from preexisting vessels and is essential in many physiologic and pathologic states, such as reproduction, development, wound healing, tumorigenesis, rheumatoid arthritis, diabetic retinopathy, and thrombosis.[1,2] Angiogenesis is tightly controlled by activators, such as fibroblast growth factors (FGFs) and vascular endothelial growth factor (VEGF), and by inhibitors, such as thrombospondin-1, interferon-α/β, platelet factor-4, and angiostatin.[3] Angiostatin was discovered in urine from mice with low-metastatic Lewis lung carcinoma as a kringle-containing fragment of plasminogen.[4] This first-reported angiostatin consists of 4 kringle domains (K1-K4) and possesses antitumor/antiangiogenic properties. Later, K1 to K3 was revealed to be a more potent inhibitor of angiogenesis.[5] Although several isoforms have been reported, angiostatin 4.5 (AS4.5, also referred to as K1-K5) is the only naturally occurring isoform identified in human plasma that consists of kringles 1 to 4 and approximately 85% of kringle 5.[6-8] Plasma concentrations of in vivo–generated AS4.5 were measured in cancer patients who received tissue plasminogen activator and mesna in a clinical trial.[9] In this study, generation of 2 isoforms of AS4.5 in human plasma was observed, namely, Lys-AS4.5 and Glu-AS4.5. Whereas Lys-AS4.5 is the originally reported natural AS4.5, Glu-AS4.5 is a larger form that obtains intact N-terminal domain of the precursor protein. Approximately 20 nM Lys-AS4.5 was detected even in the patients before treatment. After infusion of tissue plasminogen activator with mesna, Lys-AS4.5 levels increased to approximately 40 nM.

β2-glycoprotein-I (β2GPI), also known as apolipoprotein H, is a phospholipid-binding plasma protein that is one of the major autoantigens in patients with antiphospholipid syndrome, an autoimmune disorder characterized by thrombosis and pregnancy morbidity.[10-13] β2GPI is a single chain plasma glycoprotein at a concentration of approximately 4 μM composed of 5 homologous short consensus repeats, designated as domains I to V. β2GPI is cleaved by plasmin between Lys-317 and Thr-318 in domain V (nicked β2GPI), being unable to bind phospholipids.[14] This cleavage was first observed in vivo by Horbach et al[15] in plasma of patients with disseminated intravascular coagulation and in plasma with patients treated with streptokinase. In these cases, up to 12 μg/mL nicked β2GPI (~ 6% of intact β2GPI) was present. In other pathologic contexts, approximately 0.1% and approximately 1.5% of intact β2GPI are cleaved to nicked β2GPI in patients with leukemia and in patients with lupus anticoagulant, respectively.[16] In addition, in our previous study in which patients with history of stroke were investigated, up to 0.5%, mostly from 0.1% to 0.2% of intact β2GPI, was converted to nicked β2GPI in the stable state of their disease.[17] Instead of losing phospholipid-binding properties, nicked β2GPI gains the binding capacity to plasminogen and mildly suppresses the plasmin generation in the presence of tissue plasminogen activator and fibrin.[17] Because this binding is mediated by the interaction between lysine binding site on K5 of plasminogen and the lysine cluster on domain V of nicked β2GPI, we speculated on the interaction between nicked β2GPI and AS4.5, which still possesses the most part of kringle 5.

In the present study, we show that nicked β2GPI does bind AS4.5 and attenuates its antiangiogenic property in an endothelial cell proliferation assay, in an invasion assay, in a tube-formation assay, and in an in vivo angiogenesis assay.

Submitted November 27, 2008; accepted July 4, 2009. Prepublished online as *Blood* First Edition paper, July 22, 2009; DOI 10.1182/blood-2008-12-190629.

The publication costs of this article were defrayed in part by page charge payment. Therefore, and solely to indicate this fact, this article is hereby marked "advertisement" in accordance with 18 USC section 1734.

Methods

Proteins

β2GPI and nicked β2GPI were prepared as previously reported.[17] AS4.5 (K1-K5) was prepared from Glu-plasminogen (Technoclone GmbH) treated with plasmin (Calbiochem Novabiochem Corp), followed by purification steps using a lysine-Sepharose column and a Sephadex G-75 column (GE Healthcare), as previously reported.[8] Purified AS4.5 was reduced using 2-mercaptoethanol and subjected to polyacrylamide gel electrophoresis (PAGE). In some experiments, AS4.5 was treated with PNGase F or Endo H (New England Biolabs Inc) to determine whether our preparation of AS4.5 undergoes glycosylation. Purified materials were tested to exclude the possibility of lipopolysaccharide contamination using Limulus ES II Single Test (Wako).

Cells

Human aortic endothelial cells (HAECs) and human umbilical vein endothelial cells (HUVECs) were obtained from Kurabo. These cells were cultured in the moisturized chamber at 37°C with 5% CO_2, using provided cell-culture medium "EGM2" which include 2% fetal calf serum (FCS), human epidermal growth factor (10 ng/mL), human FGF-B (5 ng/mL), heparin (10 μg/mL), hydrocortisone (1 μg/mL), amphotericin B (50 ng/mL), and gentamicin (50 μg/mL). HAECs/HUVECs from 2 to 6 passages were used in the following experiments.

Kinetic assay for molecular interaction between nicked β2GPI and AS4.5

Real-time analysis for molecular interaction between intact/nicked β2GPI and AS4.5 was performed using an optical biosensor, BIACORE X (Biacore AB). Biotinylated AS4.5 was immobilized onto the streptavidin-coupled sensor chip (Biacore AB). After blocking, various concentrations (0.125, 0.25, 0.5, 1.0, and 2.0 μM) of intact or nicked β2GPI were injected and ligands bound to the surface were detected. Obtained data were used to determine the association rate constant (k_{ass}) and dissociation rate constant (k_{diss}). K_D and K_A were determined as follows: $K_D = k_{diss}/k_{ass}$ and $K_A = k_{ass}/k_{diss}$.

Inhibition ELISA

To see the fluid-phase binding between AS4.5 and nicked β2GPI, enzyme-linked immunosorbent assay (ELISA) was performed in a similar way that we previously reported.[17] Briefly, Glu-plasminogen was immobilized onto a Sumilon Type S microtiter plate (Sumitomo Bakelite). After blocking, 0.25 μM nicked β2GPI with or without AS4.5 (0.4, 0.8, or 1.6 μM) dissolved in 1% bovine serum albumin–phosphate-buffered saline (PBS) was added to the wells and plasminogen-bound nicked β2GPI molecules were detected by Cof-22 mouse monoclonal anti-β2GPI antibody.

Cell proliferation assay

To see the effect of nicked β2GPI on the proliferation of aortic endothelial cells in the presence of AS4.5, which is a potent inhibitor of endothelial cell growth, we used tetrazolium/formazan assay. After wash with PBS, 5000 HAECs in 50 μL Opti-MEM I medium (Invitrogen) were added to each wells of Celltiter 96 proliferation Assay Kit (Promega). Different concentrations of intact/nicked β2GPI with or without approximately 50 nM AS4.5 were added to the medium. After a 72-hour incubation at 37°C, 100 μL Dye Solution was added to each well and incubated for another 4 hours at 37°C. Reaction was terminated using Stop Solution and optical density at 570 nm was measured. Cell proliferation assays were also performed using HUVECs in the same manner with or without 2.5 ng/mL human recombinant VEGF (Kurabo). These assays were done in a triplicate manner for 3 times. Because the effects of intact/nicked β2GPI on HAEC proliferation and HUVEC proliferation were similar regardless of the presence or absence of AS4.5, we performed the following in vitro angiogenesis experiments using HUVECs.

Matrigel cell-invasion assay

Biocoat invasion chambers containing Matrigel-coated membranes with 8-μm pores (BD Biosciences) were used to evaluate the effect of intact/nicked β2GPI on HUVECs to migrate through a basement membrane-like extracellular matrix, in the presence or absence of AS4.5. This assay was done as previously reported, with some alterations.[18] Briefly, after removal of FCS and growth factors by washing with PBS, 5×10^4 of HUVECs in 0.5 mL Opti-MEM I medium were placed in the top chamber of each well of a 24-well culture dish. Different concentrations of intact or nicked β2GPI were applied to the top chamber in the presence or absence of AS4.5 (final concentration, ~ 50 nM). Opti-MEM I medium containing 10% FCS was added to the lower chamber of each well as chemo-attractant. After an 8-hour incubation at 37°C, the noninvading cells were removed from the top chamber and the cells that extravasated through the extracellular matrix were stained with Diff-Quick (Kokusai Shiyaku). The number of cells that migrated through the membrane's 8-μm pores were counted under Olympus IX71 inverted microscope (Olympus) equipped with a 10×/0.30 ph1 objective at a final magnification of 100×, using WinROOF image processing software (Mitani Corp). Each assay was performed in a triplicate manner 4 times.

Capillary tube formation of HUVECs cocultured with fibroblasts

The capillary tube formation of HUVECs was evaluated using an angiogenesis kit (Kurabo), according to the manufacturer's instructions. In vitro HUVEC cord formation can be observed when cocultured with human primary fibroblasts, being suitable for quantification of cumulative sprout length.[19] Evaluation of HUVEC tube formation using this coculture system is reproducible using in vitro angiogenesis kits from Kurabo or TCScell-works.[20] The culture medium in each well of a 24-well cluster dish seeded with HUVECs and human skin fibroblasts was replaced by the fresh medium containing 2.5 ng/mL human recombinant VEGF at days 1, 4, 7, and 9. We reduced the concentration of VEGF to maximize the antiangiogenic effect of AS4.5, although the recommended concentration of VEGF for the positive growth control was 10 ng/mL. At day 11, the capillary tubes formed were detected by immunostaining using anti–human CD31 antibody supplied by the manufacturer. For scoring the capillary tube formation, tube length was measured quantitatively using an Olympus IX71 inverted microscope equipped with a 4×/0.13 PhL objective and angiogenesis measuring software (KURABO Angiogenesis Image Analyzer, Version 2; Kurabo).[21] This experiment was done in a duplicate manner 3 times.

Directed in vivo angiogenesis assay

The directed in vivo angiogenesis assay was obtained from Trevigen Inc and performed as previously described,[22,23] with modifications. Briefly, sterile 0.15-cm × 1-cm-long semiclosed surgical silicone tubing (angioreactors) was filled with 18-μL high-concentration basement membrane extract, including VEGF and FGF (Trevigen Inc). Various concentrations of nicked β2GPI (0-0.4 μM) were added to angioreactors containing AS4.5. The angioreactors were then inverted and incubated at 37°C for 1 hour to allow gel formation. The angioreactors were then implanted subcutaneously into the dorsal flank of 6- to 8-week-old athymic nude female mice. Blood vessels generated in the angioreactors were quantified by staining of the recovered cell pellets with fluorescein isothiocyanate-lectin on day 10. This experiment was performed in a triplicate manner.

Statistical analysis

Statistical evaluation was performed by Student *t* test. *P* values less than .05 were considered statistically significant.

Results

Purification of nicked β2GPI and AS4.5

Purified nicked β2GPI and intact β2GPI appeared as a single band with appropriate size under sodium dodecyl sulfate-PAGE with

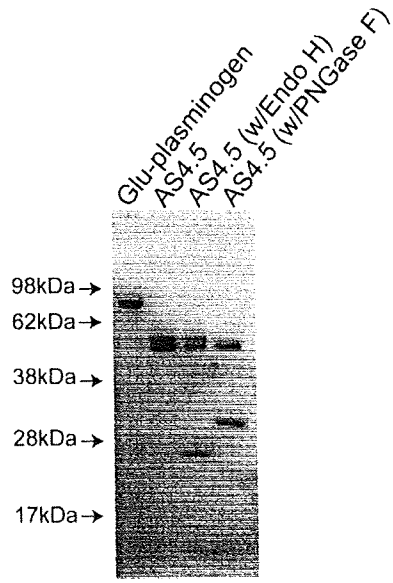

Figure 1. Preparation of nicked β2GPI and AS4.5. AS4.5 was prepared from Glu-plasminogen by plasmin digestion followed by purification using lysine-Sepharose column and Sephadex G-75 column. Purified AS4.5 was treated with PNGase F or Endo H to determine whether AS4.5 undergoes glycosylation. Glu-plasminogen, purified product (AS4.5), AS4.5 treated with PNGase F, and AS4.5 treated with Endo H were subjected to sodium dodecyl sulfate-PAGE under reduced conditions.

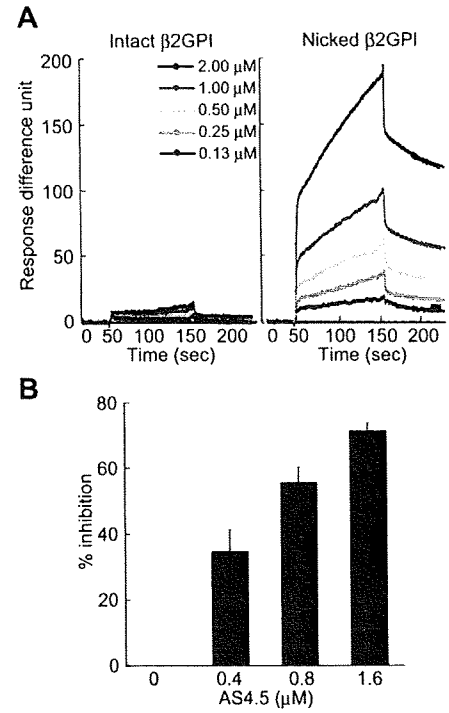

Figure 2. Binding of intact/nicked β2GPI to AS4.5. (A) Kinetic curves showing molecular interaction between AS4.5 and intact or nicked β2GPI. Intact β2GPI or nicked β2GPI binding to immobilized AS4.5 was detected using Biacore X, an optical biosensor as described in "Kinetic assay for molecular interaction between nicked B2GPI and AS4.5." Binding curve was compared between intact (left panel) and nicked β2GPI (right panel). Binding constants (K_D and K_A) between AS4.5 and nicked β2GPI were determined. (B) Binding of nicked β2GPI to immobilized Glu-plasminogen was tested in the presence or absence of AS4.5 in the fluid, using ELISA. The abilities of AS4.5 to inhibit the binding between fluid-phase nicked β2GPI and solid-phase Glu-plasminogen were shown as percentage inhibition. Error bars represent SE.

reduced conditions. Purified AS4.5 showed clear main band at expected size (52-55 kDa) with slightly larger minor band (Figure 1A). Treatment of purified AS4.5 with PNGase F resulted in the reduction of molecular weight to that of the main band, whereas treatment with Endo H had scarce effect on the size of AS4.5 (Figure 1B). According to the susceptibility to PNGase F and resistance to Endo H, at least some portion of purified AS4.5 is suggested to undergo glycosylation with complex oligosaccharides. Plasminogen undergoes glycosylation at Asn-289 and Thr-346, and additional site Leu-532, such glycosylation, can alter interaction between plasmin kringle domains and integrin αVβ3 expressed on endothelial cells.[24]

Binding of nicked β2GPI to AS4.5

Molecular interaction between intact or nicked β2GPI and AS4.5 was analyzed using an optical biosensor. Nicked β2GPI showed a large extent of binding to immobilized AS4.5, whereas intact β2GPI did not show any specific binding (Figure 2A). The data at different concentrations of nicked β2GPI were regressed, determining k_{ass} as 2.99×10^3 $M^{-1}s^{-1}$, and k_{diss} as $9.14 \times 10^{-4}s^{-1}$. Accordingly, K_D and K_A were determined as 3.05×10^{-7} M and 3.27×10^6 M^{-1}, respectively. To confirm this binding in the fluid phase, we performed inhibition ELISA. In this system, AS4.5 inhibited the binding of nicked β2GPI to immobilized Glu-plasminogen, even in the presence of excess amount of albumin (Figure 2B).

Effect of intact/nicked β2GPI on the proliferation of HAECs/HUVECs in the presence or absence of AS4.5

AS4.5 exhibited suppressive effect on the proliferation of HAECs to approximately 15% inhibition at the concentration of 50 nM, compared with the HAEC proliferation in the absence of AS4.5 (Figure 3A). In this growth factor-removed system, intact β2GPI up to the final concentration of 0.4 μM did not have any effect on the proliferation of HAECs both in the presence and absence of AS4.5. In contrast, nicked β2GPI reversed the suppressive effect on HAEC proliferation by AS4.5 (P = .021 at 0.4 μM of nicked β2GPI**, compared with the point without nicked β2GPI*). However, this form of β2GPI again had no effect on proliferation in the absence of AS4.5 at concentrations up to 0.4 μM. When HUVEC proliferation was examined in the same system, intact/nicked β2GPI exerted similar effect both in the presence and in the absence of AS4.5 (Figure 3B). When VEGF was added to this proliferation system, HUVEC proliferation was suppressed by lower concentrations of intact/nicked β2GPI in the absence of AS4.5 (Figure 3C). Suppressive effect of 50 nM AS4.5 on HUVEC proliferation was neutralized by approximately 0.1 μM nicked β2GPI. Higher concentrations (1.0-4.0 μM) of intact/nicked β2GPI suppressed HAEC/HUVEC proliferation regardless of the existence of VEGF/AS4.5 (data not shown).

Effect of intact/nicked β2GPI on the invasion of HUVECs in the presence or absence of AS4.5

Without AS4.5, intact or nicked β2GPI had no effect on the migration of HUVECs in concentrations up to 0.4 μM (Figure 4), whereas both forms of β2GPI significantly suppressed HUVEC migration in higher concentrations (from 1 to 4 μM) with dose dependency (~ 40% and 60% inhibition by 4 μM of intact and nicked β2GPI, respectively). Migration of HUVECs was down-regulated by 50 nM of AS4.5 to approximately 30% inhibition. Nicked β2GPI reversed this suppressive effect of AS4.5 at lower concentrations from 0.2 to 0.4 μM (P = .027 at 0.4 μM of nicked β2GPI**, compared with the point without nicked β2GPI*),

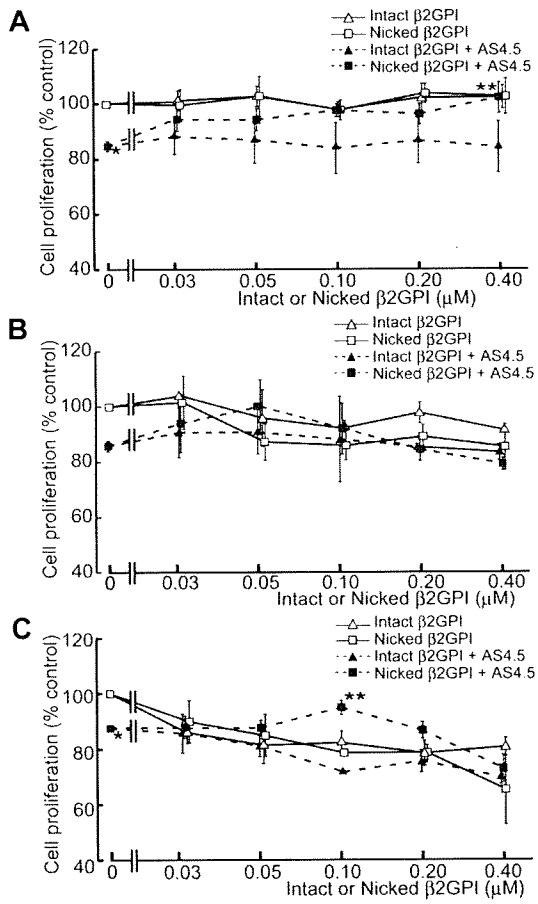

Figure 3. Effect of intact/nicked β2GPI on the proliferation of HAECs in the presence or absence of AS4.5. (A) HAECs were subjected to cell-proliferation assay using tetrazolium/formazan-based method. A total of 5000 HAECs were placed onto each wells of 96-well plate and incubated for 72 hours. The effect of serial concentrations of intact or nicked β2GPI was tested in the presence or absence of 50 nM AS4.5. HAEC proliferation in the presence of AS4.5 alone (50 nM)* was compared with that in the presence of both AS4.5 (50 nM) and nicked β2GPI (0.4 μM; **P = .021; Student t test). (B) Proliferations of HUVECs were tested using the same proliferation assay. (C) HUVEC proliferation was tested in the presence of VEGF. HUVEC proliferation in the presence of AS4.5 alone (50 nM)* was compared with that in the presence of both AS4.5 (50 nM) and nicked β2GPI (0.1 μM; **P = .030; Student t test). Error bars represent SE.

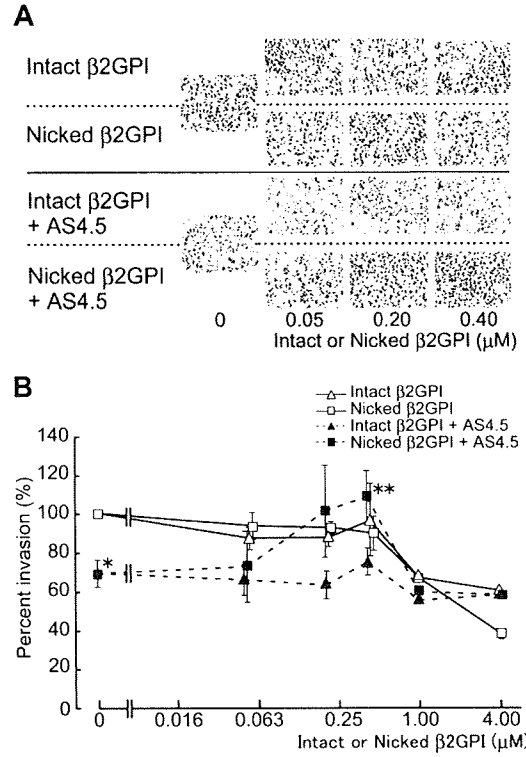

Figure 4. Effect of intact/nicked β2GPI on extravasation of HUVECs using a Matrigel-cell invasion assay in the presence or absence of AS4.5. Effect of intact or nicked β2GPI on the ability of HUVECs to migrate through a basement membrane-like extracellular matrix was evaluated in the presence or absence of AS4.5. HUVECs were added to the top wells of each chamber, and 10% FCS-enriched culture medium was added to each bottom chamber as a source of chemotactic factors. (A) In the top 2 lines of the panels, assays were done without AS4.5 AS4.5 was added to the wells in the bottom 2 lines of the panels. Serial concentrations of intact β2GPI were added in lines 1 and 3, whereas nicked β2GPI was added in lines 2 and 4. Similar results were obtained in other 3 experiments (original magnification, ×100). (B) HUVECs migrated through the Matrigel, and 8-μM pores on the membrane were stained and counted using image processing software. Ratios of the numbers of the HUVECs migrated under treatment with reagents against the number of those cells without any additional reagents were plotted on the graph. Concentrations of intact/nicked β2GPI were as follows: 0.05, 0.2, 0.4, 1.0, or 4.0 μM. Error bars represent SE. Invaded cell counts in the presence of AS4.5 alone (50 nM)* were compared with those in the presence of both AS4.5 (50 nM) and nicked β2GPI (0.4 μM; **P = .027; Student t test).

although increment of concentration diminished this reverse effect and, in turn, resulted in inhibition of HUVEC migration (~ 40% inhibition by 4 μM nicked β2GPI). Thus, depending on the concentration, nicked β2GPI shows dual effect on the mobility of HUVECs in the presence of AS4.5. Intact β2GPI had no additional or reverse effect on HUVEC migration in the presence of AS4.5 at concentrations up to 0.4 μM.

Effects of nicked β2GPI on angiogenesis (in vitro tube formation assay)

Formation of capillary-like structure by HUVECs was evaluated in the VEGF-dependent tube formation assay system. Fifty nanomolar of AS4.5 suppressed the function of HUVECs in this assay (Figure 5). Capillary tube formation was disrupted by intact β2GPI in a dose-dependent manner, in the presence or absence of AS4.5. Nicked β2GPI again reversed the inhibitory effect of AS4.5 on tube formation by HUVECs in a dose-dependent manner at concentrations up to 0.4 μM (P = .044 at 0.4 μM nicked β2GPI**, compared with the point without nicked β2GPI*). In the absence of AS4.5, nicked β2GPI had no significant effect on tube formation at concentrations less than 0.4 μM. In this assay, higher concentrations of intact/nicked β2GPI suppressed tube formation, the latter being more potent (4 μM of nicked β2GPI suppressed tube area to ~ 40 × 10^3 pixels).

Effects of nicked β2GPI on in vivo angiogenesis

Generation of blood vessels into angioreactors was suppressed by 0.2 μM AS4.5 (Figure 6). Addition of nicked β2GPI to this system up to 0.4 μM significantly recovered angiogenesis in a dose-dependent manner (P = .01).

Discussion

In the first part of this study, we demonstrated that nicked β2GPI binds AS4.5 with similar kinetics found in the interaction between nicked β2GPI and plasminogen.[17] Whereas intact β2GPI does not show any binding to plasminogen, the binding between nicked β2GPI and plasminogen was mediated via interaction between the lysine cluster of β2GPI domain V and the lysine binding site on the plasminogen K5.[17] In addition, in the present study, intact β2GPI

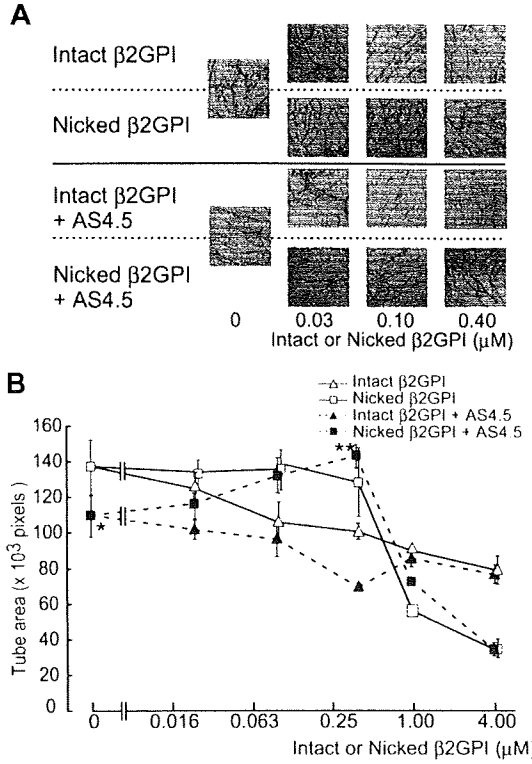

Figure 5. Effect of intact/nicked β2GPI on the VEGF-dependent tube formation of HUVECs cocultured with fibroblasts in the presence or in the absence of AS4.5. VEGF-dependent tube formation of HUVECs cocultured with primary human fibroblasts was evaluated in the presence or absence of AS4.5 (A) HUVECs were visualized by immunostaining with anti–human CD31 antibodies. In the top 2 lines of the panels, the assay was done without AS4.5 AS4.5 was added in the bottom 2 lines of the panels. Serial concentrations of intact β2GPI were added in lines 1 and 3, whereas nicked β2GPI was added in lines 2 and 4. Similar results were obtained in the second and third experiments (original magnification, ×40). (B) Capillary tube formation was quantified using KURABO Angiogenesis Image Analyzer, Version 2. Obtained data (pixels) were plotted onto the graph. Concentrations of intact/nicked β2GPI were as follows: 0.025, 0.1, 0.4, 1.0, or 4.0 μM. Error bars represent SE. Tube areas in the presence of AS4.5 alone (50 nM)* were compared with those in the presence of both AS4.5 (50 nM) and nicked β2GPI (0.4 μM; $^{**}P = .044$; Student *t* test).

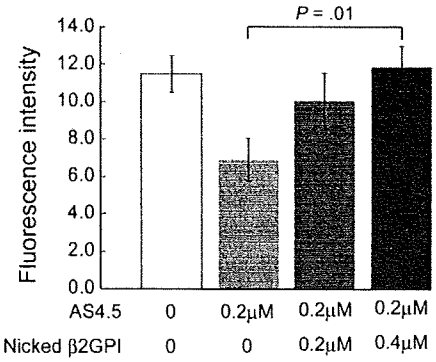

Figure 6. Nicked β2GPI suppresses the antiangiogenesis effect of AS4.5 in in vivo angiogenesis assay. Directed in vivo angiogenesis assay was performed. Semiclosed surgical silicone tubings (angioreactors) were prefilled with extracellular matrices containing VEGF and FGF alone, VEGF, FGF, and AS4.5, or VEGF, FGF, AS4.5, plus various concentrations of nicked β2GPI, then implanted subcutaneously into the dorsal flank of athymic nude mice. Blood vessels generated in the angioreactors were quantified by staining of the recovered cell pellets with fluorescein isothiocyanate-lectin. Error bars represent SE. *Fluorescence values in the presence of AS4.5 (0.2 μM) alone were compared with those in the presence of both AS4.5 and nicked β2GPI (0.4 μM) by Student *t* test ($P = .01$).

did not show any specific binding to AS4.5. This phenomenon indicates that 85% of K5 still functions enough for the binding with nicked β2GPI or that nicked β2GPI gains accessibility to other kringle domain(s) even when 15% of K5 is lost, the latter being less probable because neither K1 to K3 nor K4 disrupted the binding between nicked β2GPI and plasminogen in our previous inhibition assay.[17]

Next, we investigated the functional aspect of the interaction between nicked β2GPI and AS4.5 on the vascular endothelial cell biology. The antiangiogenic function of angiostatin is mediated by its binding onto the endothelial cell surface. Angiostatin inhibits adenosine triphosphate synthase F1F0 by direct binding to the extracellular portion of this enzyme, resulting in caspase-mediated apoptosis of endothelial cells.[25,26] Angiostatin also binds other endothelial cell surface molecules, such as integrin αVβ3 and angiomotin, although the latter binding was shown using original angiostatin K1 to K4.[27] Thus, it is speculated that nicked β2GPI interferes with the binding of AS4.5 onto the endothelial cells, resulting in attenuation of the antiangiogenic function of AS4.5. Indeed, 25 nM nicked β2GPI starts to compete with 50 nM AS4.5 and 0.1 to 0.2 μM nicked β2GPI completely abolished the antiangiogenic effect of the given AS4.5 in our HAEC proliferation assay (Figure 3A). In the HUVEC proliferation assay, 50 nM nicked β2GPI neutralized the same molar of AS4.5 (Figure 3B). In the HUVEC invasion assay and tube-formation assay, 0.1 to 0.2 μM nicked β2GPI abolished antiangiogenic properties of 50 nM AS4.5 (Figures 4,5). Based on the previous studies,[9,15,16] plasma concentrations of both nicked β2GPI and AS4.5 used in this study are physiologically available at least in thrombotic status. Moreover, it is predicted that local concentrations of nicked β2GPI and AS4.5 increase at sites of thrombosis where plasmin generation is up-regulated.

To make the situation complex, intact/nicked β2GPI itself has been reported as an inhibitor of angiogenesis. In the first report, Beecken et al[28] identified β2GPI from transitional cell carcinoma cell line, which inhibits the growth of a tumor implant in severe combined immunodeficiency mice. They demonstrated that β2GPI together with plasmin, but neither β2GPI alone nor plasmin alone, inhibits proliferation and tube formation of HUVECs, concluding that the nicked form of β2GPI is an inhibitor of angiogenesis. However, lack of using purified material makes it difficult to assume the concentration of nicked β2GPI generated in this study. Sakai et al[29] reported that 4 μM nicked β2GPI inhibited endothelial cell migration, proliferation, and neovascularization into subcutaneous implants that contain VEGF. Intraperitoneal injection of nicked β2GPI also inhibited growth of orthotopically injected tumors in a murine prostate cancer model. Only in the neovascularization study, which is a VEGF-dependent system, the same amount of intact β2GPI had similar antiangiogenic properties. Although the authors found no binding between nicked β2GPI and commercially available angiostatin (Sigma-Aldrich) using immunoprecipitation, this preparation of angiostatin does not include any portion of kringle 5. Recently, Yu et al[30] have shown that β2GPI inhibits VEGF- and FGF-induced proliferation, migration, and tube formation of HUVECs. This antiangiogenic property was found in intact β2GPI, nicked β2GPI, and also in deletion mutant lacking domain V of β2GPI, but not in β2GPI lacking domain I, concluding that this antiangiogenic property is mediated via domain I of β2GPI. This group also demonstrated that 0.5 to 2 μM intact β2GPI down-regulates mRNA expression of the VEGF receptor.

In our HAEC/HUVEC proliferation assay in which EGF and FGF were removed (Figure 3A-B), intact/nicked β2GPI had almost no effect on the proliferation of arterial endothelial cells in lower concentrations, up to 0.4 μM. Our result does not contradict that

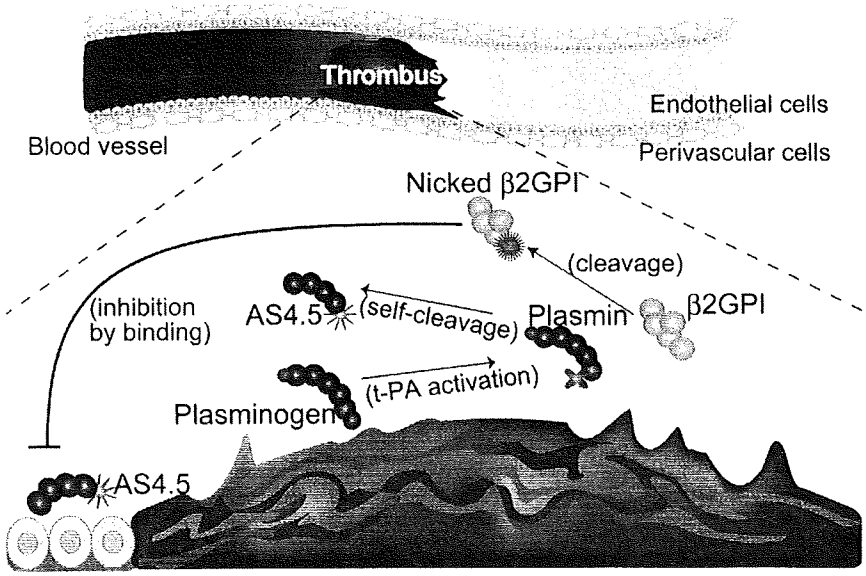

Figure 7. Beneficial effect of nicked β2GPI on thrombotic ischemia (hypothesis). (1) If thrombus is formed in the artery, up-regulation of fibrinolysis occurs and plasminogen is converted into plasmin. (2) Plasmin cleaves β2GPI into nicked β2GPI, whereas angiostatin is generated via autoproteolysis of plasminogen. (3) Nicked β2GPI binds angiostatin and attenuates its antiangiogenic property, resulting in promoted angiogenesis. tPA indicates tissue plasminogen activator.

from the Yu et al study[25] in which the antiangiogenic property of intact/nicked β2GPI was dependent on VEGF and FGF. Indeed, in our HUVEC proliferation assay with VEGF (Figure 3C) and in our VEGF-dependent tube formation assay (Figure 5), both intact and nicked β2GPI exerted antiangiogenic properties at lower concentrations. At relatively high concentrations more than 1 μM, both intact and nicked β2GPI inhibited HUVEC migration and tube formation (Figures 4B,5B), being relevant to the previous reports.[29,30] In these functional assays, nicked β2GPI exerted dual effect in the presence of AS4.5; at the lower concentrations, nicked β2GPI works as an AS4.5 inhibitor, whereas it works as an angiogenesis inhibitor at the higher concentrations. In the last part of this study, we confirmed that nicked β2GPI suppresses the antiangiogenic effect of AS4.5 in vivo (Figure 6).

Although intact β2GPI in human plasma is abundant, plasma levels of nicked β2GPI in steady-state human is up to 0.5%, 1.5% of intact form even in patients with a history of stroke[17] and those with lupus anticoagulant,[16] respectively. Thus, the antiangiogenic/antitumor effect of β2GPI in steady state is probably dependent on the intact form. On the other hand, both nicked β2GPI and angiostatin are proteolytically processed by plasmin, thus being produced at sites where fibrinolysis is up-regulated. When ischemic thrombus is formed in the artery, collateral blood flow needs to be generated by angiogenesis. In such situations, plasmin is generated, leading to the production of both nicked β2GPI and angiostatin. Those products might be stuck near the lesion resulting from the stagnant blood flow. Nicked β2GPI may exert its property as antiangiostatin in such situations, resulting in promoted angiogenesis (Figure 7). In other situations, such as tumor and diabetic retinopathy where angiostatin works beneficially, however, nicked β2GPI might be a disease-worsening factor, being a candidate for the treatment target.

In conclusion, (1) we have demonstrated the binding between nicked β2GPI and AS4.5; and (2) we propose that nicked β2GPI is a physiologic inhibitor of angiostatin both of which are produced only when fibrinolytic system is activated.

Acknowledgments

The authors thank Drs Hiroko Ogawa and Satoshi Hirohata (Department of Molecular Biology and Biochemistry, Okayama University School of Medicine) for great suggestions and discussions.

This work was supported in part by grants from the Japanese Ministry of Health, Labor and Welfare and the Japanese Ministry of Education, Culture, Sports, Science and Technology.

Authorship

Contribution: H.N. performed the research and analyzed data; S.Y. designed and performed the research and wrote the paper; E.M. and K.K. contributed analytical tools; M.I. contributed vital reagents; H.K. and T.H. analyzed data; and T.A. and T.K. wrote the paper.

Conflict-of-interest disclosure: The authors declare no competing financial interests.

Correspondence: Shinsuke Yasuda, Department of Medicine II, Hokkaido University Graduate School of Medicine, N15, W7, Kita-ku, Sapporo 060-8638, Japan; e-mail: syasuda@med.hokudai.ac.jp.

References

1. Folkman J, Shing Y. Angiogenesis. *J Biol Chem.* 1992;267(16):10931-10934.
2. Folkman J. Angiogenesis in cancer, vascular, rheumatoid and other disease. *Nat Med.* 1995; 1(1):27-31.
3. Hanahan D, Folkman J. Patterns and emerging mechanisms of the angiogenic switch during tumorigenesis. *Cell.* 1996;86(3):353-364.
4. O'Reilly MS, Holmgren L, Shing Y, et al. Angiostatin: a novel angiogenesis inhibitor that mediates the suppression of metastases by a Lewis lung carcinoma. *Cell.* 1994;79(2):315-328.
5. Cao Y, Ji RW, Davidson D, et al. Kringle domains of human angiostatin: characterization of the anti-proliferative activity on endothelial cells. *J Biol Chem.* 1996;271(46):29461-29467.
6. Gately S, Twardowski P, Stack MS, et al. The mechanism of cancer-mediated conversion of plasminogen to the angiogenesis inhibitor angiostatin. *Proc Natl Acad Sci U S A.* 1997;94(20): 10868-10872.
7. Soff GA. Angiostatin and angiostatin-related proteins. *Cancer Metastasis Rev.* 2000;19(1):97-107.
8. Cao R, Wu HL, Veitonmaki N, et al. Suppression of angiogenesis and tumor growth by the inhibitor K1-K5 generated by plasmin-mediated proteolysis. *Proc Natl Acad Sci U S A.* 1999;96(10):5728-5733.

9. Soff GA, Wang H, Cundiff DL, et al. In vivo generation of angiostatin isoforms by administration of a plasminogen activator and a free sulfhydryl donor: a phase I study of an angiostatic cocktail of tissue plasminogen activator and mesna. *Clin Cancer Res.* 2005;11(17):6218-6225.
10. Galli M, Comfurius P, Maassen C, et al. Anticardiolipin antibodies (ACA) directed not to cardiolipin but to a plasma protein cofactor. *Lancet.* 1990;335(8705):1544-1547.
11. McNeil HP, Simpson RJ, Chesterman CN, Krilis SA. Anti-phospholipid antibodies are directed against a complex antigen that includes a lipid-binding inhibitor of coagulation: β2-glycoprotein I (apolipoprotein H). *Proc Natl Acad Sci U S A.* 1990;87(11):4120-4124.
12. Matsuura E, Igarashi Y, Fujimoto M, Ichikawa K, Koike T. Anticardiolipin cofactor(s) and differential diagnosis of autoimmune disease. *Lancet.* 1990; 336(8708):177-178.
13. Hughes GR. The antiphospholipid syndrome: ten years on. *Lancet.* 1993;342(8867):341-344.
14. Hunt JE, Simpson RJ, Krilis SA. Identification of a region of β2-glycoprotein I critical for lipid binding and anti-cardiolipin antibody cofactor activity. *Proc Natl Acad Sci U S A.* 1993;90(6):2141-2145.
15. Horbach DA, van Oort E, Lisman T, Meijers JC, Derksen RH, de Groot PG. β2-glycoprotein I is proteolytically cleaved in vivo upon activation of fibrinolysis. *Thromb Haemost.* 1999;81(1):87-95.
16. Itoh Y, Inuzuka K, Kohno I, et al. Highly increased plasma concentrations of the nicked form of β2 glycoprotein I in patients with leukemia and with lupus anticoagulant: measurement with a monoclonal antibody specific for a nicked form of domain V. *J Biochem (Tokyo).* 2000;128(6):1017-1024.
17. Yasuda S, Atsumi T, Ieko M, et al. Nicked β2-glycoprotein I: a marker of cerebral infarct and a novel role in the negative feedback pathway of extrinsic fibrinolysis. *Blood.* 2004;103(10):3766-3772.
18. Yasuda S, Morokawa N, Wong GW, et al. Urokinase-type plasminogen activator is a preferred substrate of the human epithelium serine protease tryptase epsilon/PRSS22. *Blood.* 2005; 105(10):3893-3901.
19. Wenger A, Kowalewski N, Stahl A, et al. Development and characterization of a spheroidal coculture model of endothelial cells and fibroblasts for improving angiogenesis in tissue engineering. *Cells Tissues Organs.* 2005;181(2):80-88.
20. Chen Y, Wei T, Yan L, et al. Developing and applying a gene functional association network for anti-angiogenic kinase inhibitor activity assessment in an angiogenesis co-culture model. *BMC Genomics.* 2008;9:264.
21. Suzuki Y, Komi Y, Ashino H, et al. Retinoic acid controls blood vessel formation by modulating endothelial and mural cell interaction via suppression of Tie2 signaling in vascular progenitor cells. *Blood.* 2004;104(1):166-169.
22. Guedez L, Rivera AM, Salloum R, et al. Quantitative assessment of angiogenic responses by the directed in vivo angiogenesis assay. *Am J Pathol.* 2003;162(5):1431-1439.
23. Caldas H, Fangusaro JR, Boue DR, Holloway MP, Altura RA. Dissecting the role of endothelial SURVIVIN DeltaEx3 in angiogenesis. *Blood.* 2007;109(4):1479-1489.
24. Chang PC, Chang YJ, Wu HL, et al. Mutation of human plasminogen kringle 1-5 enhances antiangiogenic action via increased interaction with integrin αVβ3. *Thromb Haemost.* 2008;99(4):729-738.
25. Moser TL, Kenan DJ, Ashley TA, et al. Endothelial cell surface F1-F0 ATP synthase is active in ATP synthesis and is inhibited by angiostatin. *Proc Natl Acad Sci U S A.* 2001;98(12):6656-6661.
26. Veitonmäki N, Cao R, Wu LH, et al. Endothelial cell surface ATP synthase-triggered caspase-apoptotic pathway is essential for k1-5-induced antiangiogenesis. *Cancer Res.* 2004;64(10): 3679-3686.
27. Troyanovsky B, Levchenko T, Mansson G, Matvijenko O, Holmgren L. Angiomotin: an angiostatin binding protein that regulates endothelial cell migration and tube formation. *J Cell Biol.* 2001; 152(6):1247-1254.
28. Beecken WD, Engl T, Ringel EM, et al. An endogenous inhibitor of angiogenesis derived from a transitional cell carcinoma: clipped β2-glycoprotein-I. *Ann Surg Oncol.* 2006;13(9):1241-1251.
29. Sakai T, Balasubramanian K, Maiti S, Halder JB, Schroit AJ. Plasmin-cleaved β2-glycoprotein 1 is an inhibitor of angiogenesis. *Am J Pathol.* 2007; 171(5):1659-1669.
30. Yu P, Passam FH, Yu DM, Denyer G, Krilis SA. Beta2-glycoprotein I inhibits vascular endothelial growth factor and basic fibroblast growth factor induced angiogenesis through its amino terminal domain. *J Thromb Haemost.* 2008;6(7):1215-1223.

ARTHRITIS & RHEUMATISM
Vol. 60, No. 8, August 2009, pp 2408–2417
DOI 10.1002/art.24787

Fcγ Receptor–Dependent Expansion of a Hyperactive Monocyte Subset in Lupus-Prone Mice

Marie-Laure Santiago-Raber,[1] Hirofumi Amano,[2] Eri Amano,[2] Lucie Baudino,[1] Masako Otani,[1] Qingshun Lin,[2] Falk Nimmerjahn,[3] J. Sjef Verbeek,[4] Jeffrey V. Ravetch,[5] Yoshinari Takasaki,[2] Sachiko Hirose,[2] and Shozo Izui[1]

Objective. **Lupus-prone BXSB mice develop monocytosis characterized by selective accumulation of the Gr-1– monocyte subset. The aim of this study was to explore the possible role of activating IgG Fc receptors (FcγR) in the development of monocytosis and to characterize the functional phenotype of the Gr-1– subset that accumulates in lupus-prone mice bearing the NZB-type defective *Fcgr2b* allele for the inhibitory FcγRIIB.**

Methods. **The development of monocytosis was analyzed in BXSB and anti-IgG2a rheumatoid factor–transgenic C57BL/6 mice deficient in activating FcγR. Moreover, we assessed the expression levels of activating FcγR and inhibitory FcγRIIB on Gr-1+ and Gr-1– monocyte subsets in C57BL/6 mice bearing the C57BL/6-type or the NZB-type *Fcgr2b* allele.**

Results. **We observed monocytosis with expansion of the Gr-1– subset in anti-IgG2a–transgenic C57BL/6 mice expressing IgG2a, but not in those lacking IgG2a. Moreover, monocytosis barely developed in BXSB and anti-IgG2a–transgenic C57BL/6 mice deficient in activating FcγR. The Gr-1– subset that accumulated in lupus-prone mice displayed a unique hyperactive phenotype. It expressed very low levels of inhibitory FcγRIIB, due to the presence of the NZB-type *Fcgr2b* allele, but high levels of activating FcγRIV. This was in contrast to high levels of FcγRIIB expression and no FcγRIV expression on the Gr-1+ subset.**

Conclusion. **Our results demonstrated a critical role of activating FcγR in the development of monocytosis and in the expansion of a Gr-1– FcγRIIB^{low}FcγRIV+ hyperactive monocyte subset in lupus-prone mice. Our findings further highlight the importance of the NZB-type *Fcgr2b* susceptibility allele in murine lupus, the presence of which induces increased production of hyperactive monocytes as well as dysregulated activation of autoreactive B cells.**

The BXSB strain of mice spontaneously develops an autoimmune syndrome with features of systemic lupus erythematosus (SLE) that affects males much earlier than females (1). The accelerated development of SLE in male BXSB mice results from the genetic abnormality *Yaa* (Y-linked autoimmune acceleration), which is present on the Y chromosome in the BXSB mouse (2). Recently, the *Yaa* mutation was shown to be a consequence of a translocation from the telomeric end of the X chromosome onto the Y chromosome (3–5). Based on the presence of the gene encoding Toll-like receptor 7 (TLR-7) in this translocated segment of the X chromosome, *Tlr7* gene duplication has been proposed as the etiologic basis for *Yaa*-mediated enhancement of disease.

One of the cellular abnormalities linked to the *Yaa* mutation is monocytosis (6), which is strongly associated with autoantibody production and the subsequent development of lupus nephritis (7–9). At 8 months of age, monocytes reach a frequency of ~50% of

Supported by grants from the Swiss National Foundation for Scientific Research and the Alliance for Lupus Research.

[1]Marie-Laure Santiago-Raber, PhD, Lucie Baudino, BS, Masako Otani, MD, Shozo Izui, MD: University of Geneva, Geneva, Switzerland; [2]Hirofumi Amano, MD, PhD, Eri Amano, MD, PhD, Qingshun Lin, MD, Yoshinari Takasaki, MD, Sachiko Hirose, MD: Juntendo University School of Medicine, Tokyo, Japan; [3]Falk Nimmerjahn, PhD: University of Erlangen–Nuremberg, Erlangen, Germany; [4]J. Sjef Verbeek, PhD: Leiden University Medical Center, Leiden, The Netherlands; [5]Jeffrey V. Ravetch, MD, PhD: The Rockefeller University, New York, New York.

Drs. Santiago-Raber and Amano contributed equally to this work.

Dr. Nimmerjahn has received consulting fees, speaking fees, and/or honoraria from SuppreMol (less than $10,000).

Address correspondence and reprint requests to Shozo Izui, MD, Department of Pathology and Immunology, Centre Médicale Universitaire, 1211 Geneva 4, Switzerland. E-mail: Shozo.Izui@unige.ch.

Submitted for publication January 6, 2009; accepted in revised form May 1, 2009.

peripheral blood mononuclear cells (PBMCs) in male BXSB mice with the *Yaa* mutation. Circulating monocytes are divided into 2 phenotypically and functionally distinct subsets in mice (10,11). The first subset, which is classified as "inflammatory" monocytes and characterized by a Gr-1+CX3CR1^{low}CCR2+CD62L+ phenotype, is preferentially recruited to inflamed tissue. The second Gr-1–CX3CR1^{high}CCR2–CD62L– subset is classified as "resident" monocytes and considered to be a source of tissue-resident macrophages and dendritic cells. Significantly, monocytosis in lupus-prone mice was characterized by a selective expansion of the Gr-1– "resident" subset (12). However, the molecular basis for the development of monocytosis with expansion of the Gr-1– monocyte subset has not yet been defined.

The analysis of *Yaa* plus non-*Yaa* mixed bone marrow chimeras demonstrated no selective production of monocytes of *Yaa* origin over those of non-*Yaa* origin, thus indicating that the development of monocytosis is not due to an intrinsic abnormality in the growth potential of monocyte lineage cells from *Yaa* mice (12). Therefore, we hypothesized that *Yaa*-mediated monocytosis might result from an excessive production of a monocyte-specific growth factor(s) by macrophages due to hyperresponsiveness of their IgG Fc receptors (FcγR) to immune complexes (ICs).

It has been well established that among the 3 different types of activating FcγR expressed on murine immune effector cells, low-affinity FcγRIII and FcγRIV play a major role in the pathogenesis of IC-mediated vascular and glomerular injuries (13). However, FcγR-mediated inflammatory responses are down-regulated through coengagement of the low-affinity inhibitory FcγRIIB. Thus, competitive engagement of these 2 types of FcγR and their relative expression on immune effector cells could be critical for the development of IC-mediated inflammatory lesions in SLE. Notably, lupus-prone NZB, BXSB, and MRL strains share the NZB-type *Fcgr2b* allele (14,15), and because of deletion polymorphism in its promoter region and additional polymorphism in the putative regulatory region in intron 3 (14–17), levels of FcγRIIB expression on peritoneal macrophages in these mice were shown to be down-regulated as compared with mice carrying the B6-type *Fcgr2b* allele (9). However, it remains to be determined whether the expression levels of FcγRIIB on 2 different monocyte subsets and polymorphonuclear cells (PMNs), the immune effector cells which initially interact with circulating ICs, are similarly modulated in mice bearing the NZB-type *Fcgr2b* allele.

In the present study, we explored the possible role of activating FcγR in the development of monocytosis with expansion of the Gr-1– resident monocyte subset and characterized the functional phenotype of this subset. Our results demonstrated that the development of monocytosis and the selective expansion of the Gr-1– resident monocyte subset in lupus-prone male BXSB *Yaa* mice were dependent on IC-mediated activation of FcγR. Moreover, this subset displayed a unique hyperactive phenotype, as indicated by a very low level of expression of inhibitory FcγRIIB but a high level of expression of activating FcγRIV, in contrast to the Gr-1+ inflammatory subset, which had high expression of FcγRIIB but no expression of FcγRIV.

MATERIALS AND METHODS

Mice. C57BL/6 (B6) mice deficient in common γ-chains of the Fc receptor (FcRγ) were generated by gene targeting in B6-derived embryonic stem cells, as described previously (18). FcRγ$^{-/-}$ BXSB mice lacking expression of activating FcγRI, FcγRIII, and FcγRIV were established by selective backcrossing of (BXSB × FcRγ$^{-/-}$ B6)F$_1$ mice to BXSB mice, as described previously (19). The chromosome segment of FcRγ$^{-/-}$ B6 mice introduced into the BXSB genetic background was identified using microsatellite marker polymorphisms. (NZB × NZW)F$_1$ and B6 mice were purchased from The Jackson Laboratory (Bar Harbor, ME). FcγRIII$^{-/-}$ mice, which were generated by gene targeting in 129 mouse–derived embryonic stem cells (20), were backcrossed for 5 generations on a B6 background. FcγRIIB$^{-/-}$ mice were recently generated using B6 mouse–derived embryonic stem cells in the laboratory of one of us (JSV).

Mice expressing the 6-19 IgG3 anti-IgG2a rheumatoid factor (RF) transgene (21) were backcrossed for 8 generations on a B6 background bearing either the *Igh^a* or *Igh^b* allele. FcRγ$^{-/-}$ 6-19–transgenic mice bearing the *Igh^a* allotype were produced through intercross between corresponding B6 mice. The presence of the 6-19 transgene and the FcRγ genotype were determined by polymerase chain reaction analysis, as described previously (21,22). The expression of the *Igh^a* and *Igh^b* alleles was determined by enzyme-linked immunosorbent assay (ELISA), as described elsewhere (23).

Animal studies were approved by the Ethical Committee for Animal Experimentation, Faculty of Medicine, University of Geneva.

Flow cytometric analysis. Flow cytometry was performed using 3-color or 4-color staining of peripheral blood cells and analyzed with a FACSCalibur instrument (BD Biosciences, San Jose, CA). The following antibodies were used: M1/70 anti-CD11b, anti-F4/80, anti–Gr-1, AFS98 anti-CD115 (macrophage colony-stimulating factor receptor) (24), K9.361 anti-Ly17.2 (B6-type FcγRIIB), 9E9 anti-FcγRIV (25), 2.4G2 anti-FcγRIIB/III, and RA3-6B2 anti-B220 monoclonal antibodies (mAb).

The mean ± SD percentage of CD11b+F4/80+ monocytes (distinguished from PMNs by their lower level of granularity, as reflected in a low side light–scatter pattern) among PBMCs in 8-month-old male B6 mice (n = 15) was 10.3 ±

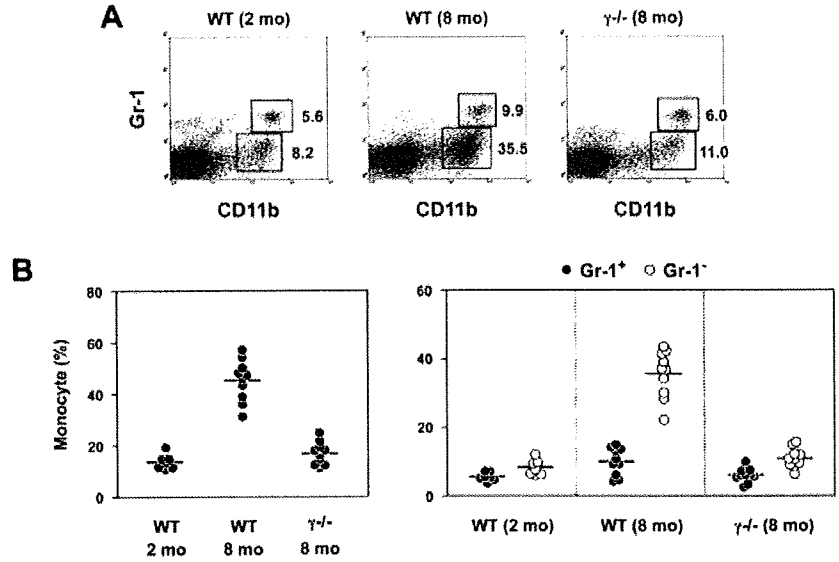

Figure 1. Suppression of both monocytosis and expansion of the Gr-1– subset in male FcR$\gamma^{-/-}$ BXSB *Yaa* mice. **A,** Peripheral blood mononuclear cells (PBMCs) from male wild-type (WT) and FcR$\gamma^{-/-}$ ($\gamma^{-/-}$) BXSB *Yaa* mice at 2 and 8 months of age were stained with a combination of anti-CD11b and anti–Gr-1 monoclonal antibodies (mAb). PBMCs were gated for cells with lower granularity (low side light–scatter properties) to distinguish them from polymorphonuclear cells. Representative staining profiles for Gr-1 and CD11b on PBMCs are shown. Numbers indicate the mean percentages of Gr-1+ and Gr-1– monocytes (n = 7–10 mice per group). **B,** PBMCs from the same groups of mice were stained with a combination of anti-CD11b, anti-F4/80, and anti–Gr-1 mAb. Shown are the percentages of CD11b+F4/80+ monocytes (left) and Gr-1+ and Gr-1– CD11b+ monocyte subsets (right) in individual mice in each group. Horizontal bars show the mean. Differences in the percentages of monocytes between male WT and FcR$\gamma^{-/-}$ BXSB *Yaa* mice and between Gr-1+ and Gr-1– subsets in male BXSB *Yaa* mice at 8 months of age were highly significant ($P < 0.0001$).

3.0%. Mice displaying percentages of monocytes that were more than 3SD above the mean in male B6 mice (>19.3%) were considered to be positive for monocytosis.

Serologic assays. Serum levels of gp70–anti-gp70 ICs and IgG3 anti-IgG2a RF were determined by ELISA, as described previously (8,26). Cryoglobulins were isolated from sera as described elsewhere (26). Concentrations of IgG2a and IgG2c in cryoglobulins were determined by ELISA using polyclonal goat anti-IgG2a antibodies that were cross-reactive with IgG2c (SouthernBiotech, Birmingham, AL) by referring to standard curves established with serum pools from B6 mice bearing either the Igh^a or Igh^b allotype.

In vitro binding of IgG2a ICs to monocytes. IgG2a ICs were prepared in vitro by incubation of fluorescein isothiocyanate (FITC)–labeled Hy1.2 IgG2a anti-dinitrophenyl (anti-DNP) mAb (50 μg/ml) and DNP15–bovine serum albumin (DNP15-BSA; 50 μg/ml) at 37°C for 2 hours. Then, PBMCs from B6 mice were incubated with a mixture of FITC-labeled Hy1.2 mAb plus DNP15-BSA or FITC-labeled Hy1.2 mAb alone in the presence of either hamster 9E9 FcγRIV-blocking mAb (25) or polyclonal hamster IgG (Jackson ImmunoResearch Europe, Suffolk, UK) as a control. The cells were simultaneously stained with phycoerythrin-labeled anti–Gr-1 and biotinylated AFS98 anti-CD115 mAb, followed by staining with allophycocyanin. Binding of FITC-labeled Hy1.2 mAb on Gr-1+ and Gr-1– monocytes was analyzed with a FACSCalibur instrument.

Statistical analysis. Analyses for percentages of monocytes and their subsets were performed with the Mann-Whitney U test. Unpaired comparison of the mean fluorescence intensity (MFI) of 9E9 and 2.4G2 staining of monocyte subsets was analyzed by Student's *t*-test. Probability values >5% were considered insignificant.

RESULTS

Suppression of monocytosis and of the expansion of the Gr-1– subset in lupus-prone male BXSB *Yaa* mice deficient in FcRγ. As described previously (6,12), 8-month-old male BXSB *Yaa* mice developed monocytosis, with 31–57% of PBMCs being CD11b+F4/80+ monocytes (mean ± SD 45.3 ± 8.1%) and a predominance of the Gr-1– resident subset (Figure 1). However, when the development of monocytosis was assessed in male FcRγ-deficient BXSB *Yaa* mice lacking the func-

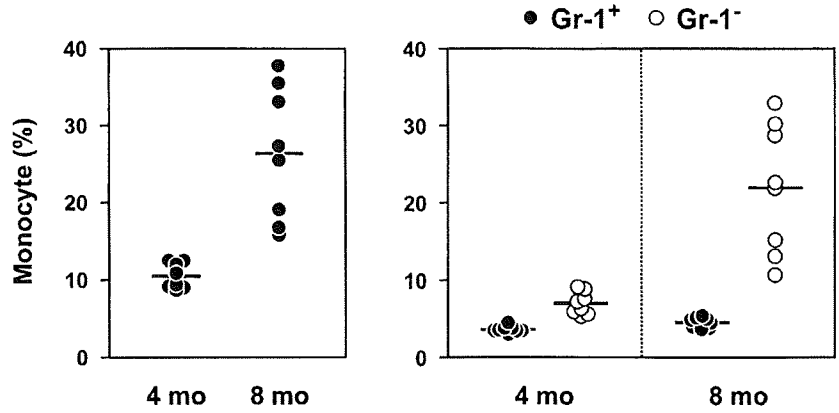

Figure 2. Development of monocytosis with expansion of the Gr-1– monocyte subset in (NZB × NZW)F_1 mice. Peripheral blood mononuclear cells from 4-month-old and 8-month-old female (NZB × NZW)F_1 mice were stained with a combination of anti-CD11b, anti-F4/80, and anti–Gr-1 monoclonal antibodies. Shown are the percentages of CD11b+F4/80+ monocytes (left) and Gr-1+ and Gr-1– CD11b+ monocyte subsets (right) in individual mice in each group (n = 8 mice per group). Horizontal lines show the mean.

tional expression of all 3 activating receptors (FcγRI, FcγRIII, and FcγRIV), neither monocytosis nor expansion of the Gr-1– monocyte subset was observed at 8 months of age (Figure 1). Notably, as shown previously (19), male FcRγ-deficient BXSB *Yaa* mice still developed high titers of IgG anti-DNA autoantibodies and nephritogenic gp70–anti-gp70 ICs at levels comparable with those in male wild-type (WT) BXSB *Yaa* mice (data not shown). These results indicated that the development of monocytosis and expansion of the Gr-1– subset in aged BXSB *Yaa* mice resulted from FcγR-dependent activation of immune effector cells by the accumulation of ICs in lupus-prone mice.

Development of monocytosis with expansion of the Gr-1– monocyte subset in lupus-prone (NZB × NZW)F_1 mice. The implication of FcγR in monocytosis occurring in BXSB *Yaa* mice prompted us to explore the possible development of monocytosis in (NZB × NZW)F_1 mice, another lupus-prone strain. Percentages of monocytes in the peripheral blood were only slightly increased in female (NZB × NZW)F_1 mice at 4 months of age (mean ± SD 10.5 ± 1.6%) (Figure 2). In contrast, at 8 months of age, 5 of the 8 mice displayed significant increases in monocytes, with a mean value of 26.4 ± 8.6% ($P < 0.001$). Although the extent of monocytosis was moderate as compared with that in male BXSB *Yaa* mice (Figure 1B), monocytosis occurring in aged female (NZB × NZW)F_1 mice was characterized by a selective increase in the Gr-1– monocyte subset (4.5 ± 0.7% Gr-1+ monocytes and 21.9 ± 8.3% Gr-1– monocytes) (Figure 2), as was the case in male BXSB *Yaa* mice.

FcγR-dependent monocytosis with expansion of the Gr-1– monocyte subset in 6-19 IgG3 anti-IgG2a RF–transgenic mice. The role of IgG ICs and activating FcγR in the development of monocytosis was further examined in B6 mice expressing the 6-19 IgG3 anti-IgG2a RF transgene and bearing either the Igh^a or Igh^b allele. Since 6-19 RF is specific for IgG2a (but not IgG2c), 6-19 IgG3–IgG2a ICs were only formed in B6.Igh^a 6-19–transgenic mice, which express IgG2a, but not in conventional B6 mice, which bear the Igh^b allele, an allele that expresses IgG2c, but not IgG2a. This finding was confirmed by the presence of IgG2a, but not IgG2c, in 6-19 cryoglobulins isolated from the sera of B6.Igh^a and B6 (Igh^b) 6-19–transgenic mice (data not shown), since 6-19 mAb generated cryoglobulins because of the unique physicochemical property of the IgG3 subclass (21,27).

At 3–4 months of age, all B6.Igh^a 6-19–transgenic mice developed monocytosis (mean ± SD 27.6 ± 5.7%), whereas none of the B6 (Igh^b) 6-19–transgenic mice displayed monocytosis (10.6 ± 0.8%; $P < 0.0001$) (Figure 3). Again, the development of monocytosis in B6.Igh^a 6-19–transgenic mice was due to an accumulation of the Gr-1– monocyte subset (6.2 ± 2.1% Gr-1+ monocytes and 21.9 ± 5.6% Gr-1– monocytes) (Figure 3). Furthermore, the implication of activating FcγR in the development of monocytosis was confirmed by the absence of monocytosis in FcRγ$^{-/-}$ B6.Igh^a 6-19–transgenic mice (Figure 3). It should also be mentioned that the extent of monocytosis in B6.Igh^a 6-19–

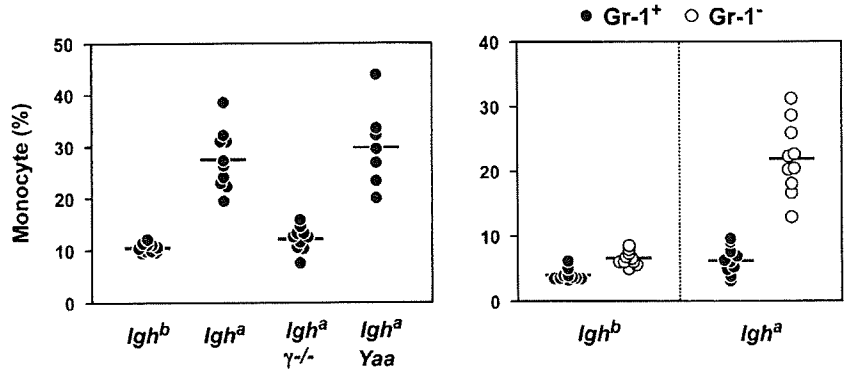

Figure 3. Fcγ receptor (FcγR)–dependent monocytosis with expansion of the Gr-1– monocyte subset in 6-19 anti-IgG2a rheumatoid factor (RF)–transgenic B6 mice. Peripheral blood mononuclear cells (PBMCs) from 6-19 anti-IgG2a RF–transgenic mice were stained with a combination of anti-CD11b, anti-F4/80, and anti–Gr-1 monoclonal antibodies. Shown are the percentages of CD11b+F4/80+ monocytes in PBMCs from 3–4-month-old 6-19 anti-IgG2a–transgenic mice of 4 different genotypes: those bearing the Igh^b allotype (n = 10 female mice), those bearing the Igh^a allotype (n = 10 female mice), those bearing the Igh^a allotype and deficient in FcR γ-chains (Igh^a $\gamma^{-/-}$; n = 10 female mice) and those bearing the Igh^a allotype and the *Yaa* mutation (Igh^a *Yaa*; n = 7 male mice) (left), as well as the percentages of Gr-1+ and Gr-1– CD11b+ monocyte subsets in PBMCs from 6-19–transgenic mice bearing either the Igh^b or Igh^a allotype (n = 10 female mice per group) (right) in individual mice in each group. Horizontal lines show the mean. Notably, serum levels of transgenic IgG3 anti-IgG2a RF activities in B6.Igh^a 6-19–transgenic mice were comparable with those in FcR$\gamma^{-/-}$ or *Yaa*-bearing B6.Igh^a–transgenic mice (data not shown).

transgenic mice was not exacerbated by the presence of the *Yaa* mutation (Figure 3).

Selective expression of activating FcγRIV on Gr-1–, but not Gr-1+, monocyte subsets and higher capacity of Gr-1– than Gr-1+ monocytes for binding to IgG2a ICs in B6 mice. It has been shown that the monocytes that repopulated the circulation after monocyte depletion by liposome treatment were exclusively of the Gr-1+ subset (11) and that these cells were the only monocytes initially labeled after in vivo treatment with bromodeoxyuridine (12). These results support the idea that Gr-1+ and Gr-1– monocytes represent 2 different stages of maturation in the bloodstream. To determine the possible functional differences between Gr-1+ and Gr-1– monocytes, we compared the expression levels of low-affinity FcγR (FcγRIIB, FcγRIII, and FcγRIV), all of which efficiently bind circulating ICs. The expression of FcγRIIB and FcγRIV on monocytes was assessed with B6-type FcγRIIB-specific K9.361 and with FcγRIV-specific 9E9 mAb, respectively, whereas the expression of FcγRIII was evaluated by the staining of FcγRIIB-deficient monocytes with 2.4G2 anti-FcγRIIB/III mAb because of the lack of FcγRIII-specific mAb.

The extent of surface staining for FcγRIIB and for FcγRIII on Gr-1+ monocytes in B6 mice was comparable and slightly higher, respectively, as compared with their staining on Gr-1– monocytes (Figure 4A). In contrast, FcγRIV was expressed only on the Gr-1– subset, and not on the Gr-1+ subset. These data suggested that Gr-1– monocytes that newly express FcγRIV could more efficiently interact with IgG2a ICs than Gr-1+ monocytes. Indeed, the binding analysis of in vitro–prepared IgG2a ICs between Hy1.2 anti-DNP mAb and DNP15-BSA revealed a higher capacity of Gr-1– monocytes than Gr-1+ monocytes to bind to IgG2a ICs (Figure 4B). This enhanced binding was no longer observed in the presence of 9E9 FcγRIV–blocking mAb, thereby confirming the implication of FcγRIV in an increased IgG IC–binding activity of Gr-1– monocytes.

Very low level of expression of inhibitory FcγRIIB on the Gr-1–FcγRIV+ monocyte subset in B6 mice bearing the NZB-type *Fcgr2b* allele. We have previously shown that the expression of FcγRIIB on resident peritoneal macrophages from B6 mice bearing the NZB-type *Fcgr2b* allele, which is shared by lupus-prone mice (14–16), was markedly diminished as compared with that from conventional B6 mice bearing the B6-type *Fcgr2b* allele (9). Since our analysis showed comparable expression of the B6-type FcγRIIB allelic form on Gr-1+ and Gr-1– monocytes in B6 mice (Figure 4A), we compared the expression levels of FcγRIIB on

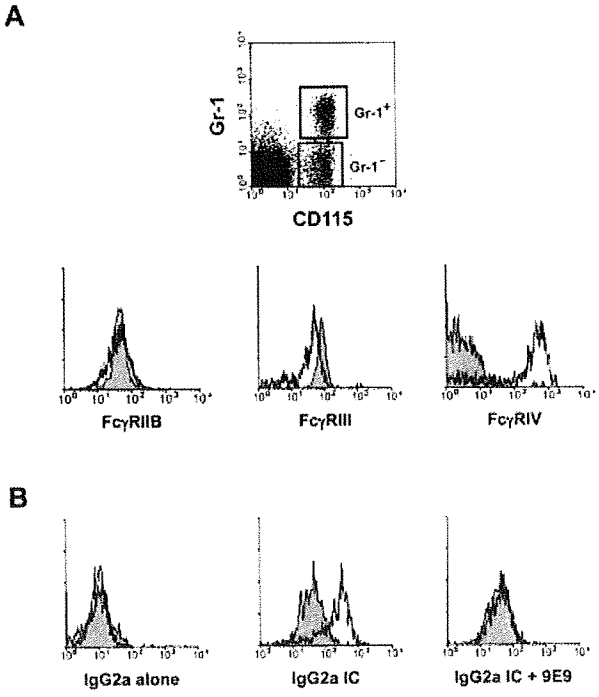

Figure 4. Selective expression of activating Fcγ receptor IV (FcγRIV) on Gr-1– monocytes and higher capacity of Gr-1– monocytes than Gr-1+ monocytes for binding to IgG2a immune complexes (ICs) in B6 mice. **A,** Peripheral blood mononuclear cells (PBMCs) from 2–3-month-old female B6 mice were stained with a combination of anti-CD115, anti–Gr-1, and 1 of 3 different anti-FcγR monoclonal antibodies (mAb) and were then gated for CD115+ cells to define the expression levels of FcγRIIB, FcγRIII, and FcγRIV on Gr-1+ and Gr-1– monocytes (top). Histograms show the expression levels of FcγRIIB and FcγRIV on Gr-1+ (shaded) and Gr-1– (thick line) CD115+ monocytes, as determined using B6-type FcγRIIB allele–specific K9.361 and FcγRIV-specific 9E9 mAb, respectively, as well as of FcγRIII, as determined by staining of FcγRIIB-deficient monocytes with 2.4G2 anti-FcγRIIB/III mAb (bottom). Results are representative of the findings in 3–5 mice. **B,** PBMCs from 2–3-month-old female B6 mice were incubated with preformed IgG2a ICs, consisting of fluorescein isothiocyanate (FITC)–labeled Hy1.2 IgG2a anti-dinitrophenyl (anti-DNP) mAb plus DNP15–bovine serum albumin (DNP15-BSA), or with FITC-labeled Hy1.2 mAb alone, in the absence or presence of hamster 9E9 FcγRIV–blocking mAb and were then stained with anti-CD115 and anti–Gr-1 mAb. Histograms show the binding of Hy1.2 IgG2a on Gr-1+ (shaded) and Gr-1– (thick line) CD115+ monocytes. Results are representative of the findings in 3 mice.

these 2 subsets of monocytes in B6 mice with the NZB-type *Fcgr2b* allele. Because of the lack of a mAb that was able to specifically recognize the NZB-type allelic form of FcγRIIB, we used 2.4G2 anti-FcγRIIB/III mAb to determine the expression levels of FcγRIIB on monocytes from FcγRIII$^{-/-}$ B6 mice carrying the 129-derived NZB-type *Fcgr2b* allele, which was cotransferred with the *Fcgr3* mutant gene during backcrossing of the mutated 129 interval to B6 mice (9).

Flow cytometric analysis of FcγRIII$^{-/-}$ monocytes revealed that the expression level of FcγRIIB on Gr-1– monocytes was much lower than that on Gr-1+ monocytes, whereas both Gr-1+ and Gr-1– subsets in FcRγ$^{-/-}$ B6 mice carrying the B6-type *Fcgr2b* allele stained equally with the 2.4G2 mAb (Figure 5A). Notably, a similar down-regulated expression of FcγRIIB was observed on PMNs bearing the NZB-type *Fcgr2b* allele, but not on circulating B cells (Figure 5B). These data indicated a selective down-regulation of the expression of FcγRIIB on Gr-1–FcγRIV+ monocytes and PMNs bearing the NZB-type *Fcgr2b* allele as compared with those bearing the B6-type *Fcgr2b* allele.

Selective expansion of FcγRIIB^{low}FcγRIV+ monocytes in aged BXSB mice bearing the NZB-type *Fcgr2b* allele. To confirm that Gr-1– monocytes accumulating in aged male BXSB *Yaa* mice bearing the NZB-type *Fcgr2b* allele indeed displayed the FcγRIIB^{low}FcγRIV+ phenotype, the expression levels of FcγRIV and FcγRIIB were determined by flow cytometric analysis. As expected, Gr-1– monocytes from 8-month-old male BXSB *Yaa* mice with monocytosis highly expressed FcγRIV on their surface (mean ± SD MFI 327.2 ± 28.1; n = 3 mice) at levels comparable with those on Gr-1– monocytes from B6 mice (MFI 362.3 ± 42.5; n = 5 mice) (Figure 5C). Although the expression of FcγRIIB could not be directly determined because of the lack of antibodies specific for the NZB-type FcγRIIB allelic form, the majority of Gr-1– monocytes displayed limited staining with 2.4G2 anti-FcγRIIB/III mAb, as compared with the Gr-1+ subset. Notably, 2.4G2 staining of Gr-1– monocytes from BXSB mice (MFI 39.4 ± 13.4) was clearly weaker than that of Gr-1– monocytes from B6 mice (MFI 74.2 ± 4.6; $P < 0.005$), whereas Gr-1+ monocytes displayed comparable MFI of 2.4G2 staining in both strains of mice (MFI 115.9 ± 28.7 in BXSB mice and 144.7 ± 10.7 in B6 mice). Collectively, our data suggested that Gr-1– FcγRIIB^{low}FcγRIV+ monocytes accumulated in the peripheral blood of male BXSB *Yaa* mice as a result of exposure of IgG ICs during the course of the disease.

DISCUSSION

The present study was designed to define the molecular mechanisms responsible for the development of monocytosis, which is characterized by a selective expansion of the Gr-1– monocyte subset in lupus-prone BXSB *Yaa* mice. Analysis of BXSB *Yaa* and 6-19 anti-IgG2a–transgenic B6 mice deficient in activating

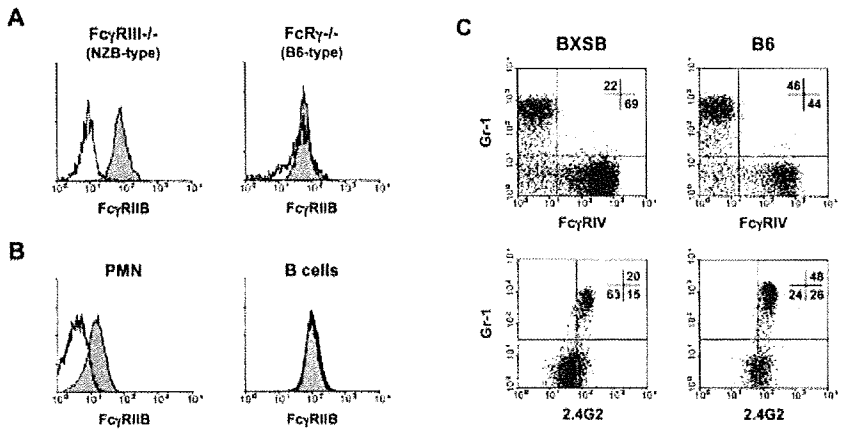

Figure 5. Very low level of expression of inhibitory Fcγ receptor IIB (FcγRIIB) on the Gr-1– monocyte subset and polymorphonuclear cells (PMNs) from B6 mice bearing the NZB-type *Fcgr2b* allele and selective expansion of FcγRIIB^{low}FcγRIV+ monocytes in aged BXSB mice bearing the NZB-type *Fcgr2b* allele. **A,** Peripheral blood mononuclear cells (PBMCs) from 2–3-month-old female FcγRIII$^{-/-}$ and FcRγ$^{-/-}$ B6 mice bearing the NZB-type and B6-type *Fcgr2b* allele, respectively, were stained with a combination of anti-CD115, anti–Gr-1, and 2.4G2 anti-FcγRIIB/III monoclonal antibodies (mAb). Histograms show the expression levels of FcγRIIB on Gr-1+ (shaded) and Gr-1– (thick line) CD115+ monocytes, as determined by staining of FcγRIII-deficient and FcRγ$^{-/-}$ monocytes with 2.4G2 anti-FcγRIIB/III mAb. Results are representative of the findings in 3 mice. **B,** PMNs and circulating B cells from 2–3-month-old female FcγRIII$^{-/-}$ and FcRγ$^{-/-}$ B6 mice bearing the NZB-type and B6-type *Fcgr2b* allele, respectively, were stained with a combination of anti-CD115, anti–Gr-1, anti-B220, and 2.4G2 anti-FcγRIIB/III mAb. Histograms show the expression levels of FcγRIIB on Gr-1^{high}CD115– PMNs (distinguished from Gr-1+ monocytes by their much higher expression of Gr-1 and higher granularity, as reflected in high side light–scatter properties) and B220+ B cells bearing the NZB-type (thick line) and B6-type *Fcgr2b* (shaded) allele. Results are representative of the findings in 3 mice. **C,** PBMCs from 8-month-old male BXSB *Yaa* and B6 *Yaa* mice were stained with a combination of anti-CD115, anti–Gr-1, 9E9 anti-FcγRIV, and 2.4G2 anti-FcγRIIB/III mAb, and gated for CD115+ monocytes. Representative staining profiles for FcγRIV and FcγRIIB/III on Gr-1+ and Gr-1– monocytes are shown. Numbers indicate the mean percentages of Gr-1+FcγRIV– and Gr-1–FcγRIV+ monocytes, as well as of Gr-1+2.4G2^{high}, Gr-1–2.4G2^{low}, and Gr-1–2.4G2^{high} monocytes (n = 3–5 mice per group).

FcγR demonstrated that the development of monocytosis was a consequence of IC-triggered activation of immune effector cells, such as monocyte/macrophages, through activating FcγR. Moreover, the Gr-1– monocyte subset accumulating in BXSB *Yaa* mice bearing the NZB-type *Fcgr2b* allele, which is common in lupus-prone mice, was revealed to display a hyperactive phenotype in response to IgG ICs because of low expression of inhibitory FcγRIIB but high expression of activating FcγRIV.

Our previous analysis of *Yaa* plus non-*Yaa* mixed bone marrow chimeras showed that there was no selective production of monocytes of *Yaa* origin over those of non-*Yaa* origin (12). This result suggests that monocytosis associated with the *Yaa* mutation is a result of excessive production of monocyte-specific growth factors by immune effector cells in response to ICs during the course of lupus-like autoimmune disease. Indeed, the absence of monocytosis in male BXSB *Yaa* mice deficient in activating FcγR, despite high production of autoantibodies (19), indicates that IC-mediated, FcγR-dependent activation of immune effector cells is crucial for the development of monocytosis. This conclusion was further supported by 2 findings. First, the expression of the 6-19 IgG3 anti-IgG2a RF transgene induced monocytosis only in B6 mice expressing IgG2a, but not in those deficient in activating FcγR or lacking IgG2a. Second, the development of monocytosis was also observed in (NZB × NZW)F_1 mice, another lupus-prone strain, at 8 months of age, when high titers of autoantibodies started to accumulate.

In light of these results, it seems plausible that

persistent FcγR-mediated activation of monocyte/macrophages by IgG ICs may result in the production of excessive amounts of monocyte-specific growth factors, thereby leading to the development of monocytosis. Notably, interactions of IgG ICs with FcγR on macrophages trigger the production of macrophage colony-stimulating factor and granulocyte–macrophage colony-stimulating factor by macrophages (28,29).

It should be stressed that the extent of monocytosis in (NZB × NZW)F_1 mice and in 6-19 anti-IgG2a RF–transgenic B6 mice was less severe than that observed in BXSB *Yaa* mice. This indicates that the *Yaa* mutation somehow plays a unique role in the development of monocytosis. The recently identified *Tlr7* gene duplication resulting from a translocation from the telomeric end of the X chromosome (containing the *Tlr7* gene) onto the Y chromosome has been proposed as the etiologic basis for *Yaa*-mediated enhancement of SLE (3–5). Accordingly, the development of monocytosis was strongly suppressed in B6 *Yaa* mice congenic for the *Nba2* (NZB autoimmunity 2) locus following the introduction of the *Tlr7*-null mutation on the X chromosome (30). This suggests that IgG ICs containing endogenous nuclear antigens could excessively activate *Yaa*-bearing macrophages through interaction with FcγR and then with TLR-7, which is expressed at increased levels in endosomes of these macrophages, to secrete high levels of monocyte-specific growth factors. In addition, because of the *Tlr7* gene duplication, the *Yaa* mutation selectively enhances the production of autoantibodies against nuclear antigens that are capable of interacting with TLR-7, thereby further promoting the activation of *Yaa*-bearing macrophages (3–5,30,31). This is consistent with the finding that the presence of the *Yaa* mutation failed to aggravate the extent of monocytosis in 6-19 IgG3 anti-IgG2a–transgenic mice, since IgG3–IgG2a ICs are not expected to interact with TLR-7.

Analysis of $FcR\gamma^{-/-}$ BXSB mice and 6-19 anti-IgG2a–transgenic B6 mice revealed that IC-mediated, FcγR-dependent activation was also responsible for an expansion of the Gr-1– subset, 1 of the 2 major monocyte subsets that are present in the circulation. Since recent immigrants from bone marrow appear to enter the circulation as Gr-1+ monocytes (11,12), it has been suggested that the Gr-1+ subset consecutively becomes the Gr-1– subset while still in the bloodstream. In this regard, our demonstration that activating FcγRIV was expressed on the Gr-1– subset, but not on the Gr-1+ subset, supports the idea that the Gr-1– subset represents a more mature stage of monocytes as compared with the Gr-1+ subset, although this has not yet been formally proven. The selective accumulation of the Gr-1– subset in lupus-prone mice developing monocytosis is likely to be due to a longer half-life of the Gr-1– subset as compared with that of the Gr-1+ subset (10,11).

It is significant that the Gr-1– monocyte subset that accumulated in lupus-prone mice carried a unique functional phenotype, since it expressed very low levels of inhibitory FcγRIIB but high levels of activating FcγRIV, in contrast to the high levels of FcγRIIB and no FcγRIV expression on the Gr-1+ monocyte subset. It has been well established that the relative balance of engagement of activating and inhibitory FcγR is critical for the development of IC-mediated tissue lesions (13). Thus, it is reasonable to assume that the Gr-1– monocyte subset accumulating in lupus-prone mice could be excessively activated in the presence of circulating IgG ICs, thereby actively participating in the development and progression of IC-mediated tissue injury in SLE.

Previous reports have shown a considerable role of infiltrating monocyte/macrophages in the progression of glomerular lesions (32) and of FcγR in glomerulonephritis, including murine lupus nephritis (18,33,34). Thus, monocytosis could actively participate in the development of glomerular inflammation and injury through increased secretion of proinflammatory cytokines, reactive oxygen species, and matrix-specific proteases as a result of IC-mediated, FcγR-dependent activation of infiltrating monocyte/macrophages. Moreover, down-regulated expression of FcγRIIB on PMNs bearing the NZB-type *Fcgr2b* allele could additionally contribute to the development of glomerular lesions in lupus-prone mice, since a considerable role of PMNs in IC-mediated inflammatory disorders has been well established (35,36).

The findings of our study further underline the importance of the NZB-type *Fcgr2b* allele as a lupus susceptibility gene in murine SLE. The down-regulated expression of FcγRIIB on monocyte/macrophages, PMNs, as well as activated B cells in lupus-prone mice appears to contribute not only to increased production of autoantibodies as a result of dysregulated activation of autoreactive B cells (19,37), but also to enhanced IC-mediated glomerular and vascular inflammation as a result of excessive activation of monocyte/macrophages and PMNs. The selective expression of FcγRIV on Gr-1– resident monocytes in mice appears to have an analogy in humans, since FcγRIIIA, the human homolog of FcγRIV (38), is expressed on the resident, but not the inflammatory, subset in humans (39). In view of the critical role of FcγR and the accumulation of a

hyperactive monocyte subset in parallel with the progression of disease in lupus-prone mice, the enumeration of blood monocytes and the analysis of their subsets, especially the FcγRIIB^{low}FcγRIIIA+ subset, might be useful predictive markers in patients with SLE.

ACKNOWLEDGMENTS

We thank Dr. T. Moll for critical reading of the manuscript, and Mr. G. Celetta, Mr. G. Brighouse, and Mr. G. Sealy for excellent technical help.

AUTHOR CONTRIBUTIONS

All authors were involved in drafting the article or revising it critically for important intellectual content, and all authors approved the final version to be published. Dr. Izui had full access to all of the data in the study and takes responsibility for the integrity of the data and the accuracy of the data analysis.

Study conception and design. Santiago-Raber, H. Amano, Hirose, Izui.

Acquisition of data. Santiago-Raber, H. Amano, E. Amano, Baudino, Otani.

Analysis and interpretation of data. Santiago-Raber, H. Amano, E. Amano, Baudino, Otani, Hirose, Izui.

Generation of FcRγ$^{-/-}$ BXSB mice. Lin, Hirose.

Provision of anti-FcγRIV monoclonal antibody. Nimmerjahn, Ravetch.

Provision of FcγRIIB$^{-/-}$ and FcγRIII$^{-/-}$ mice. Verbeek.

REFERENCES

1. Murphy ED, Roths JB. A Y chromosome associated factor in strain BXSB producing accelerated autoimmunity and lymphoproliferation. Arthritis Rheum 1979;22:1188–94.
2. Izui S, Iwamoto M, Fossati L, Merino R, Takahashi S, Ibnou-Zekri N. The Yaa gene model of systemic lupus erythematosus. Immunol Rev 1995;144:137–56.
3. Pisitkun P, Deane JA, Difilippantonio MJ, Tarasenko T, Satterthwaite AB, Bolland S. Autoreactive B cell responses to RNA-related antigens due to TLR7 gene duplication. Science 2006;312: 1669–72.
4. Subramanian S, Tus K, Li QZ, Wang A, Tian XH, Zhou J, et al. A Tlr7 translocation accelerates systemic autoimmunity in murine lupus. Proc Natl Acad Sci U S A 2006;103:9970–5.
5. Deane JA, Pisitkun P, Barrett RS, Feigenbaum L, Town T, Ward JM, et al. Control of Toll-like receptor 7 expression is essential to restrict autoimmunity and dendritic cell proliferation. Immunity 2007;27:801–10.
6. Wofsy D, Kerger CE, Seaman WE. Monocytosis in the BXSB model for systemic lupus erythematosus. J Exp Med 1984;159: 629–34.
7. Kofler R, McConahey PJ, Duchosal MA, Balderas RS, Theofilopoulos AN, Dixon FJ. An autosomal recessive gene that delays expression of lupus in BXSB mice. J Immunol 1991;146:1375–9.
8. Merino R, Fossati L, Lacour M, Lemoine R, Higaki M, Izui S. H-2-linked control of the Yaa gene-induced acceleration of lupus-like autoimmune disease in BXSB mice. Eur J Immunol 1992;22: 295–9.
9. Kikuchi S, Santiago-Raber ML, Amano H, Amano E, Fossati-Jimack L, Moll T, et al. Contribution of Nba2 to Yaa-induced monocytosis in association with murine systemic lupus. J Immunol 2006;176:3240–7.
10. Geissmann F, Jung S, Littman DR. Blood monocytes consist of two principal subsets with distinct migratory properties. Immunity 2003;19:71–82.
11. Sunderkotter C, Nikolic T, Dillon MJ, Van Rooijen N, Stehling M, Drevets DA, et al. Subpopulations of mouse blood monocytes differ in maturation stage and inflammatory response. J Immunol 2004;172:4410–7.
12. Amano H, Amano E, Santiago-Raber ML, Moll T, Martinez-Soria E, Fossati-Jimack L, et al. Selective expansion of a monocyte subset expressing the CD11c dendritic cell marker in the Yaa model of systemic lupus erythematosus. Arthritis Rheum 2005;52: 2790–8.
13. Nimmerjahn F, Ravetch JV. Fcγ receptors: old friends and new family members. Immunity 2006;24:19–28.
14. Jiang Y, Hirose S, Abe M, Sanokawa-Akakura R, Ohtsuji M, Mi X, et al. Polymorphisms in IgG Fc receptor IIB regulatory regions associated with autoimmune susceptibility. Immunogenetics 2000; 51:429–35.
15. Pritchard NR, Cutler AJ, Uribe S, Chadban SJ, Morley BJ, Smith KG. Autoimmune-prone mice share a promoter haplotype associated with reduced expression and function of the Fc receptor FcγRII. Curr Biol 2000;10:227–30.
16. Xiu Y, Nakamura K, Abe M, Li N, Wen XS, Jiang Y, et al. Transcriptional regulation of Fcgr2b gene by polymorphic promoter region and its contribution to humoral immune responses. J Immunol 2002;169:4340–6.
17. Rahman ZS, Manser T. Failed up-regulation of the inhibitory IgG Fc receptor FcγRIIB on germinal center B cells in autoimmune-prone mice is not associated with deletion polymorphisms in the promoter region of the FcγRIIB gene. J Immunol 2005;175: 1440–9.
18. Park SY, Ueda S, Ohno H, Hamano Y, Tanaka M, Shiratori T, et al. Resistance of Fc receptor-deficient mice to fatal glomerulonephritis. J Clin Invest 1998;102:1229–38.
19. Lin Q, Xiu Y, Jiang Y, Tsurui H, Nakamura K, Kodera S, et al. Genetic dissection of the effects of stimulatory and inhibitory IgG Fc receptors on murine lupus. J Immunol 2006;177: 1646–54.
20. Hazenbos WL, Gessner JE, Hofhuis FM, Kuipers H, Meyer D, Heijnen IA, et al. Impaired IgG-dependent anaphylaxis and Arthus reaction in FcγRIII (CD16) deficient mice. Immunity 1996;5:181–8.
21. Kikuchi S, Pastore Y, Fossati-Jimack L, Kuroki A, Yoshida H, Fulpius T, et al. A transgenic mouse model of autoimmune glomerulonephritis and necrotizing arteritis associated with cryoglobulinemia. J Immunol 2002;169:4644–50.
22. Azeredo da Silveira S, Kikuchi S, Fossati-Jimack L, Moll T, Saito T, Verbeek JS, et al. Complement activation selectively potentiates the pathogenicity of the IgG2b and IgG3 isotypes of a high affinity anti-erythrocyte autoantibody. J Exp Med 2002;195: 665–72.
23. Merino R, Iwamoto M, Fossati L, Muniesa P, Araki K, Takahashi S, et al. Prevention of systemic lupus erythematosus in autoimmune BXSB mice by a transgene encoding I-E α chain. J Exp Med 1993;178:1189–97.
24. Sudo T, Nishikawa S, Ogawa M, Kataoka H, Ohno N, Izawa A, et al. Functional hierarchy of c-kit and c-fms in intramarrow production of CFU-M. Oncogene 1995;11:2469–76.
25. Nimmerjahn F, Bruhns P, Horiuchi K, Ravetch JV. FcγRIV: a novel FcR with distinct IgG subclass specificity. Immunity 2005; 23:41–51.
26. Berney T, Fulpius T, Shibata T, Reininger L, Van Snick J, Shan H, et al. Selective pathogenicity of murine rheumatoid factors of the cryoprecipitable IgG3 subclass. Int Immunol 1992;4:93–9.
27. Abdelmoula M, Spertini F, Shibata T, Gyotoku Y, Luzuy S, Lambert PH, et al. IgG3 is the major source of cryoglobulins in mice. J Immunol 1989;143:526–32.

28. Thorens B, Mermod JJ, Vassalli P. Phagocytosis and inflammatory stimuli induce GM-CSF mRNA in macrophages through posttranscriptional regulation. Cell 1987;48:671–9.
29. Hora K, Satriano JA, Santiago A, Mori T, Stanley ER, Shan Z, et al. Receptors for IgG complexes activate synthesis of monocyte chemoattractant peptide 1 and colony-stimulating factor 1. Proc Natl Acad Sci U S A 1992;89:1745–9.
30. Santiago-Raber ML, Kikuchi S, Borel P, Uematsu S, Akira S, Kotzin BL, et al. Evidence for genes in addition to Tlr7 in the Yaa translocation linked with acceleration of systemic lupus erythematosus. J Immunol 2008;181:1556–62.
31. Christensen SR, Shupe J, Nickerson K, Kashgarian M, Flavell RA, Shlomchik MJ. Toll-like receptor 7 and TLR9 dictate autoantibody specificity and have opposing inflammatory and regulatory roles in a murine model of lupus. Immunity 2006;25:417–28.
32. Wenzel U, Schneider A, Valente AJ, Abboud HE, Thaiss F, Helnchen UM, et al. Monocyte chemoattractant protein-1 mediates monocyte/macrophage influx in anti-thymocyte antibody-induced glomerulonephritis. Kidney Int 1997;51:770–6.
33. Clynes R, Dumitru C, Ravetch JV. Uncoupling of immune complex formation and kidney damage in autoimmune glomerulonephritis. Science 1998;279:1052–4.
34. Kaneko Y, Nimmerjahn F, Madaio MP, Ravetch JV. Pathology and protection in nephrotoxic nephritis is determined by selective engagement of specific Fc receptors. J Exp Med 2006;203:789–97.
35. Coxon A, Cullere X, Knight S, Sethi S, Wakelin MW, Stavrakis G, et al. FcγRIII mediates neutrophil recruitment to immune complexes: a mechanism for neutrophil accumulation in immune-mediated inflammation. Immunity 2001;14:693–704.
36. Tsuboi N, Asano K, Lauterbach M, Mayadas TN. Human neutrophil Fcγ receptors initiate and play specialized nonredundant roles in antibody-mediated inflammatory diseases. Immunity 2008;28:833–46.
37. McGaha TL, Sorrentino B, Ravetch JV. Restoration of tolerance in lupus by targeted inhibitory receptor expression. Science 2005;307:590–3.
38. Mechetina LV, Najakshin AM, Alabyev BY, Chikaev NA, Taranin AV. Identification of CD16-2, a novel mouse receptor homologous to CD16/FcγRIII. Immunogenetics 2002;54:463–8.
39. Passlick B, Flieger D, Ziegler-Heitbrock HW. Identification and characterization of a novel monocyte subpopulation in human peripheral blood. Blood 1989;74:2527–34.